DATA-BASED QUANTIFICATION OF PROCESS NONLINEARITY

MASTER OF SCIENCE IN ENGINEERING

(CHEMICAL)

MALIK MOHAMMAD TAHIYAT

Department of Chemical Engineering

Bangladesh University of Engineering and Technology, Dhaka

August 2015

DATA-BASED QUANTIFICATION OF PROCESS NONLINEARITY

by

MALIK MOHAMMAD TAHIYAT

A thesis submitted to the Department of Chemical Engineering

in partial fulfillment of the requirements for the degree of

MASTER OF SCIENCE IN ENGINEERING

(CHEMICAL)

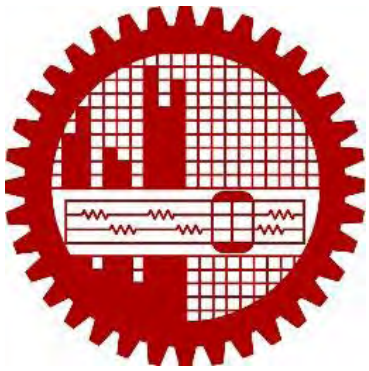

Department of Chemical Engineering

Bangladesh University of Engineering and Technology, Dhaka

ABSTRACT

The field of quantification of nonlinearity has drawn much attention from researchers in recent times. However, the scope of research on quantification of nonlinearity, especially for process plants, remains a vast area to explore. Nonlinearity in process plants may arise from two factors, namely, instruments and process characteristics. Instruments can induce nonlinearity due to their nonlinear dynamics or faults such as stiction, hysteresis and saturation. Process may themselves be nonlinear in nature or may show nonlinear behavior due to violation of some physical limits or constraints. Nonlinearity quantifications are useful for many purposes such as checking the adequacy of a linear controller for a nonlinear process and finding the root cause of a fault that arose due to increase in nonlinearity of the instruments. Model based quantification of nonlinearity is difficult, expensive and time consuming. On the other hand, data-based nonlinearity quantification methods are easy to use and becoming popular due to readily available data from Distributed Control System (DCS) or data historian of the plants.

Four data-based nonlinearity measures, namely, Bicoherence based, Surrogate Data based, Correlation Dimension and Maximal Lyapunov Exponent are studied and their performances are compared in this thesis. Both simulations and experimental investigations have been undertaken to compare and find the suitability of the data-based nonlinearity measures for quantification of nonlinearity for chemical processes. Bicoherence-based measure was found to be the most successful among them and the Surrogate data-based measure was next to it.

ACKNOWLEDGMENTS

The author expresses his sincere thanks to Prof. Dr. M. A. A. Shoukat Choudhury, Head of Department, Department of Chemical Engineering, Bangladesh University of Engineering and Technology (BUET), for proposing the present research topic. The author would also like to express his profound respect to him for the valuable guidance and supervision throughout the entire work.

The author is grateful for support and suggestions from Mr Md Aminul Islam Khan, doctoral candidate, Memorial University of Newfoundland, regarding this research work.

The author would also like to gratefully acknowledge Mr Rajesh Paul, Lecturer, Department of Chemical Engineering, BUET, for his cooperation with some of the programming intricacies.

Acknowledgments are also made for the help rendered by the staff of the Department of Chemical Engineering, BUET.

Financial support in the form of scholarship for the author from BUET Chemical Engineering Forum (BCEF) is gratefully acknowledged

CONTENTS

LIST OF FIGURES

LIST OF TABLES

CHAPTER 1

INTRODUCTION

Study of Nonlinear systems have been of foremost interest to researchers because most physical systems in reality are nonlinear. Nonlinear systems are defined by those, which do not follow the principle of superposition. Nonlinearities in process variables can be caused by valve stiction (acronym of 'static friction'), hysteresis in valves or instruments, deadzone, etc., which, in turn, sets up oscillations that may propagate throughout the whole plant. For nonlinear plants, linear controllers such as PID controllers may not perform well. Therefore, quantification of nonlinearity may help in deciding whether to implement linear or nonlinear controllers.

Two broad approaches exist for measuring nonlinearity of a process: Model based measures (also termed 'parametric') and Time-series or Data-based measures (also termed 'non-parametric'). The preference of the Data-based approaches over the Model-based resides on the fact that Model-based approaches, like Best Linear Approximation and Curvature-Based methods, require a process model which is often unavailable or diffi-

cult to obtain [3]. Therefore, in recent times, data-based methods are gaining popularity because they require time series data of the process which are readily available from the Distributed Control System (DCS) or data historian. Most notable data-based methods include Bicoherence-Based Measures, [2, 7], Surrogate Data-based Measures [21, 38], Correlation dimension and maximal Lyapunov Exponent [40, 41].

1.1 Linear and Nonlinear Systems

When a process system is linear, it follows the principle of superposition, which is given by the following two equations:

$$Additivity : f(x+y) = f(x) + f(y) \tag{1.1}$$

$$Homogeneity : f(\alpha x) = \alpha f(x), where\ \alpha\ is\ a\ constant. \tag{1.2}$$

In a linear process, if the input is reduced by x, the effect on the output will be exactly opposite but of the same magnitude to an increase in x in the input [26]. For a nonlinear control system, these conditions do not hold true. The response and behavior of the system changes with time and load applied to the system. It needs to be retuned regularly while a linear system may be tuned once and may stay tuned forever if the process does not change.

Generally linear systems have the following characteristics:

1. All dependent variables are continuous i.e. they give a continuous response over the range of values exhibited by the system.

2. All coefficients of the differential equations, which characterize the system, are constants or functions of time only.

3. When several inputs are applied at the same or different locations at the same or a different time, the total response is the sum of the individual responses (superposition).

4. Magnitude of the output is directly proportional to the magnitude of the input.

Nonlinear systems do not have one or more of these characteristics. Typical nonlinear systems include operation in saturation zones for actuators, piping network (arising due to dynamic friction losses in the piping network as they vary with respect to square of the flow rate), Heat Exchanger system and Acid-base titration system.

In general, the linear system theory is more mature, and the development, implementation, and maintenance costs of linear controller are usually lower than those of nonlinear controller for the same process [6]. Therefore, linearization is a primary approach used for most nonlinear processes [8, 9, 36].

1.2 Nonlinearities in Process Industries

Some cases of nonlinearities that are generally observed in the process industry are discussed in this section.

1.2.1 Nonlinearity in Flow Sensor

In case of an orifice-type flow-sensor, the actual measurement (Pressure-drop across the orifice plate) has a square relationship to the desired measurement (flow through the orifice meter). A square root, which is a nonlinear function, must be extracted of the directly measured data before the signal becomes usable [23].

1.2.2 Nonlinearities in Petrochemical Industry

Petrochemical processes are invariably described by nonlinear thermodynamics and kinetic models. These models are hard to formulate primarily because the feedstocks in the units are not well characterized and the physical parameters are hard to identify. Therefore, in addition to the model parameters being uncertain, these models are nonlinear.

Several nonlinear control responses exist in a fractionation process. Examples include the flow of steam to reboilers being controlled by regulating steam condensate withdrawal from the reboiler calandria. Steam flow can be reduced only after a significant delay to allow condensate to accumulate and partially flood the calandria. Energy control is sluggish and nonlinear because it is easier to drain condensate from the reboiler receiver than it is to condense the steam. Nonlinear reboiler and reflux accumulator level control responses can also be observed in these processes especially when the reboilers use overflow weir design [11].

1.2.3 Nonlinearities in pH Process

Control of waste water pH has two characteristics: nonlinearity and a large control action range. These characteristics distinguish it from most of the other control loops. By definition, one unit of pH refers to 10-fold change in concentration of hydrogen cations. Thus for a strong-acid strong-base, a single unit change in pH requires a 10-fold change in reagent flow. The titration curve in Figure 1.1 shows that the open-loop gain at pH=7 is much greater than the open-loop gain at ph=12, thus rendering the process a nonlinear one [11].

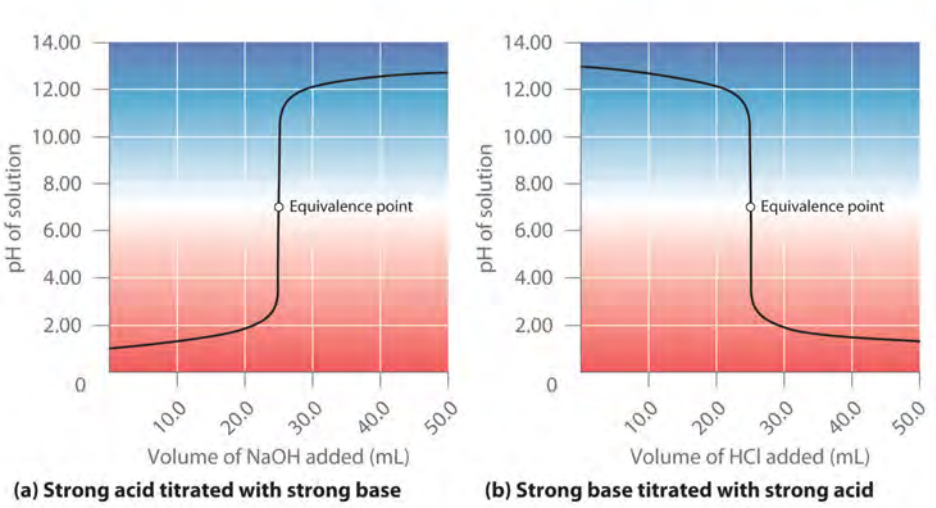

Figure 1.1: Strong Acid- Strong Base Titration Curve

1.2.4 Actuator Nonlinearities

Control Valve may exhibit nonlinearity of saturation type when the valve is either fully opened or fully closed. The valve with linear characteristics may behave in a linear

fashion as long it does not saturate. Considering Nonlinearity is thus important when large changes are made in valve position. Nonlinearity should also be taken into account during start-up and shutdown [1].

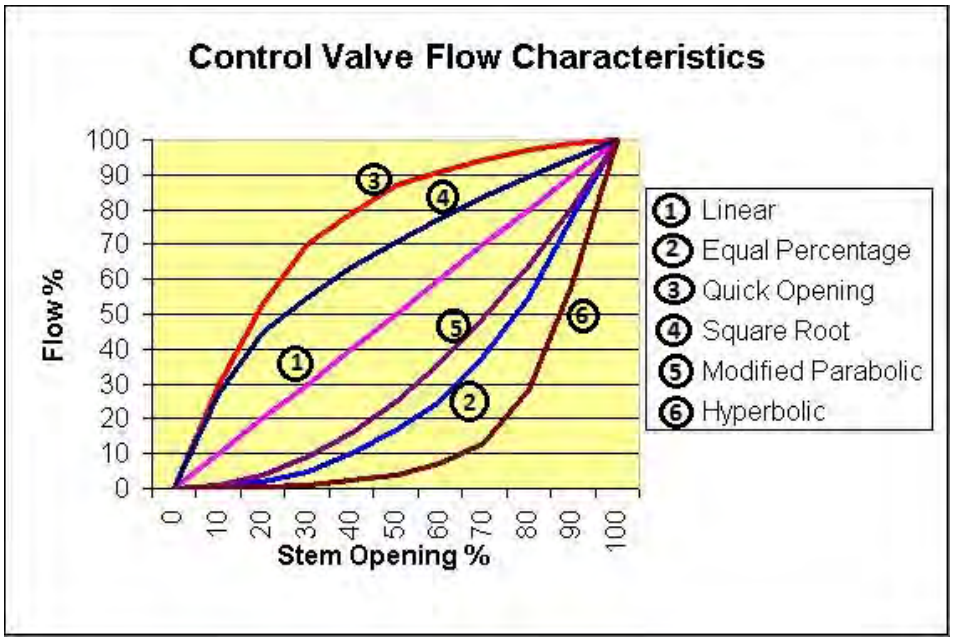

Figure 1.2: Control Valve Flow Characteristics

Figure 1.2 shows nonlinear characteristics of some control valves. These include equal percentage, quick opening, square-root, modified parabolic and hyperbolic characteristics. They are nonlinear because their gain changes for large changes in stem opening.

Usually the signal sent to the actuator and the process measurement are used as input-output data pair for parameter estimation. But inherent actuator nonlinearities may result in a poor model and thus wrong control. For a known nonlinearity (e.g. Square law relationship) [18], it is advantageous to cascade an inverse nonlinearity to

make the process as linear as possible. Such compensation will greatly increase the robustness of the estimator. Other nonlinearities like static friction, hysteresis, and nonlinear gain of the actuator can be reduced by a local feedback such as valve positioner control or flow control where possible [27].

1.3 Objectives of the Study

This work will evaluate the performance of various data-based measures of nonlinearity using simulation and experimental study in order to find their suitability in quantifying nonlinearity of chemical processes. The study will focus mainly on the investigation of the suitability of various nonlinearity measures in quantifying nonlinearity and compare their performances.

1.4 Thesis Organization

The first chapter of this thesis briefly introduces 'Nonlinearity' and its presence in process industry. It also describes the motivations for this research and objectives of the study.

Chapter 2 briefly describes the role of 'Nonlinearity Measures' and their literature review.

Chapter 3 discusses four data-based nonlinearity measures, which are used throughout the thesis for quantification of nonlinearity.

Chapter 4 evaluates the performance of nonlinearity measures on analytical signals and several nonlinear mathematical functions.

Chapter 5 discusses two nonlinear processes, which are modeled using MATLAB and SIMULINK. Then output time series data from these processes are used for nonlinearity quantification.

Chapter 6 discusses the effect of feedback controller on process nonlinearities.

Chapter 7 discusses an experimental study using a nonlinear tank with a conical bottom. The water level data is recorded by manipulating the input flow-rate of water. The output time series data of the water level, obtained from the experiment, is studied for nonlinearity quantification.

The thesis ends with Chapter 8, which lists conclusions and recommendations for future work.

CHAPTER 2

LITERATURE REVIEW

Process nonlinearity is one of the most relevant factors in characterizing process control problems. In recent years several approaches have been proposed to assess nonlinearity of static systems as well as dynamic systems [15]. The nonlinearity, as an inherent feature of industrial processes, can influence the operating performance significantly. From the control loop perspective, plants and actuators are two main parts, in which nonlinear characteristics exist. But the respective nonlinearity of each part cannot be isolated and measured when the entire system is running together. Thus, the nonlinear test of the entire system is usually performed.

Research has predominantly treated open-loop input-output (I/O) systems in the vicinity of some stationary operating point either through nonlinearity tests or through nonlinearity measures. Nonlinearity tests are well known in the field of system identification [13]. They evaluate the deviation from a property which is known to hold for linear systems. Nonlinearity measures are a means of quantifying the 'degree' of

nonlinearity in the I/O behavior of nonlinear systems. Such measures allow a direct comparison of the nonlinearity of different processes or different operating points of a single process. Although the strict mathematical definition of linearity is a definite true/false property, it is sometimes interesting to study whether a system is closer to being 'linear' or 'nonlinear' [36]. Some of the noticeable researches involving nonlinearity measures are discussed here.

There are two broad approaches for nonlinearity quantification- namely, model based methods and data-driven methods.

2.1 Model Based Methods

2.1.1 Minimum Variance Lower Bound Ratio

Generally, the closed loop nonlinearity measures require complicated mathematical knowledge and detailed process information. To improve the practicality in industrial field, a closed-loop nonlinearity measure, which belongs to the data-driven class and is based on minimum variance lower bound ratio is proposed in [24]. This measure does not need the input/output map as prior knowledge and has no effect on the routine operation. This measure, can be estimated from the routine operating data, and can be used for Hammerstein structure, Wiener structure and Wiener-Hammerstein structure. The method assumes that the system output can be expressed as the sum of a disturbance term and a nonlinear term. However, this measure is prone to modeling errors.

As shown in Figure 2.1a, r is the set-point, er_t is the control error, u_t is the output

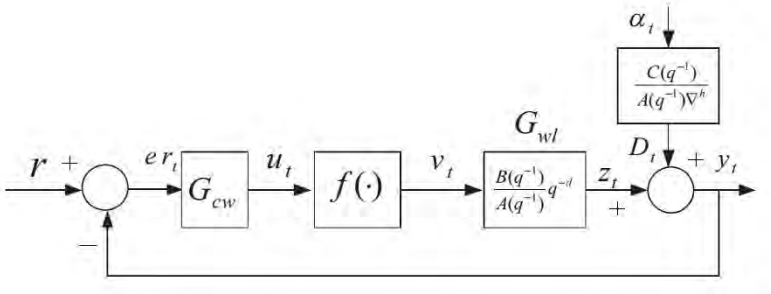

(a) The Hammerstein structure of the closed loop system

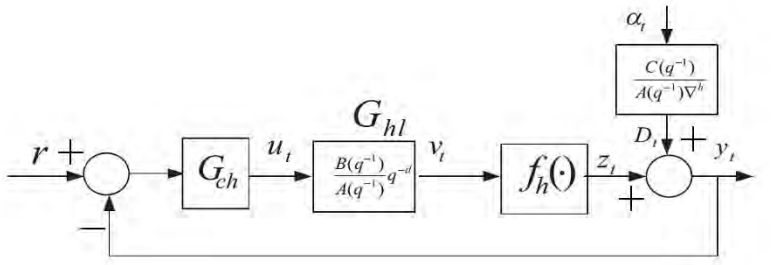

(b) The Weiner structure of the closed loop system

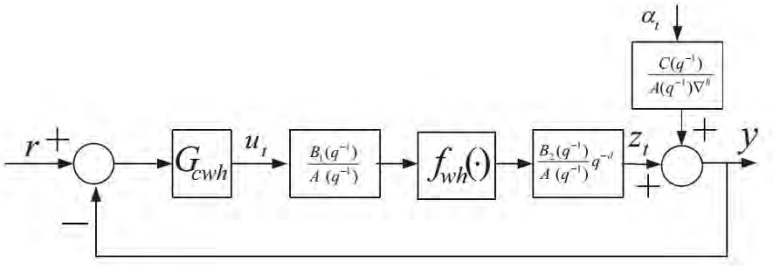

(c) The Weiner-Hammerstein structure of the closed loop system

Figure 2.1: Hammerstein, Weiner and Weiner-Hammerstein structures of closed loop system [24].

of controller G_{cw}, ν_t is the output of the nonlinear function $f(\cdot)$, and α_t is a zero-mean white noise with variance δ_α^2. G_{wl} is the linear dynamic with the time delay, d, $A(q^1)$ and $B(q^{-1})$ are the polynomials, describing process dynamics. Disturbance, D_t, is defined

as a linear Autoregressive Integrated Moving Average (ARIMA) where, $C(q^{-1})$ is the polynomial in the backshift operator q^{-1}, $\bigtriangledown$ is $(1 - q^{-1})$ and y_t is the output of the system.

The b-step ahead prediction value of y_t is given by:

$$y_{t+b} = \frac{B(q^{-1})}{A(q^{-1})} f(u_t) + D_{t+b|t} + e_{t+b|t} \tag{2.1}$$

where $D_{t+b|t}$ is the b-step ahead prediction value of disturbance and $e_{t+b|t}$ is the b-step ahead prediction error of the output. The nonlinear minimum variance lower bound can be written as

$$\delta^2_{mv} = var(e_{t+b|t}) \tag{2.2}$$

After linearization, b-step ahead prediction value of y_t is changed as:

$$y_{t+b} = \frac{B(q^{-1})}{A(q^{-1})} l(u_t) + D_{t+b|t} + e_{t+b|t} + \mu_t \tag{2.3}$$

where μ_t is the bias of linear approximation error. Therefore, the estimation of the linear minimum variance lower bound can be calculated as

$$\widetilde{\delta}^2_{mv} = var(e_{t+b|t} + \mu_t) \tag{2.4}$$

A normal Nonlinearity measure is defined as

$$\eta = 1 - \frac{\delta^2_{mv}}{\widetilde{\delta}^2_{mv}} \tag{2.5}$$

With modifications of G_{cw}, this measure can be applied to the other two structures. η is bounded in [0,1] where 0 represents no nonlinearity and 1 represents the strongest nonlinearity.

2.1.2 Linear Approximation

A model based nonlinearity measure based on best linear approximation for dynamic systems was proposed in [15]. An approximate computational strategy transferring the original infinite-dimensional nested optimization problem into a convex finite-dimensional minimization problem is discussed. The measure provides a unifying framework for nonlinearity assessment of

- Analysis of Steady state operating points of continuously operated processes
- Trajectory-dependent analysis of batch or other transient processes

But application examples have been restricted to operating point dependent analysis of stationary processes since in such analysis, the initial conditions are known for the nonlinear and linear system.

The nonlinearity measures $\phi_N^{y_a}$ of a nonlinear dynamic system $N : \mathcal{U}_a \times \mathcal{X}_{0,a} \to \mathcal{Y}$ with output signals $\mathbf{y}_N \in \mathcal{Y}_a \subseteq \mathcal{Y}$ is defined by the non-negative number:

$$\phi_N^{y_a}(t_f) = \inf_{G \in \mathcal{G}} \sup_{(\mathbf{u}, \mathbf{x}_{N,0}) \in \mathcal{S}} \inf_{\mathbf{x}_{G,0} \in \mathcal{X}_{0,G}} \frac{\|G[\mathbf{u}, \mathbf{x}_{G,0}] - N[\mathbf{u}, \mathbf{x}_{N,0}]\|}{\|N[\mathbf{u}, \mathbf{x}_{N,0}]\|} \tag{2.6}$$

with $\mathcal{S} = \{(\mathbf{u}, \mathbf{x}_{N,0}) : \mathbf{u} \in \mathcal{U}_a, \mathbf{x}_{N,0} \in \mathcal{X}_{0,a}, N[\mathbf{u}, \mathbf{x}_{N,0}] \in \mathcal{Y}_a\}$

where $G : U_a \times \mathcal{X}_{0,G} \to \mathcal{Y}$ is a linear dynamic operator belonging to the space of linear operators $\mathcal{G}$. $\mathcal{U}_a, \mathcal{X}_{0,a}, \mathcal{Y}_a$ are the spaces of admissible inputs, initial conditions, and outputs, respectively, $\|.\|$ is a suitable norm in $\mathcal{Y}$. All signals and norms are defined over a (finite or infinite) time interval $[0, t_f]$. The existence of $\mathbf{y}$ and the boundedness of all norms in the above definition are assumed for all $(\mathbf{u}, \mathbf{x}_{N,0}) \subseteq S$. For analysis during

stable operating points, the inner inf-operator is left out and $x_{G,0}$ is set to zero.

$$\phi_{OP}^{y_a} = \inf_{G \in \mathcal{G}} \sup_{u \in \mathcal{U}_a} \frac{\|G[\mathbf{u}, \mathbf{0}] - N[\mathbf{u}, \mathbf{x}_{N,s}]\|}{\|N[\mathbf{u}, \mathbf{x}_{N,s}]\|} \tag{2.7}$$

The above definition of nonlinearity for a dynamic system is defined as the normalized largest difference between the nonlinear process and a linear time-invariant system. This difference is calculated for the best linear approximation G^* of N with respect to the "worst-case" combination of inputs $\mathbf{u}^*$ and initial conditions $\mathbf{x}_{N,0}^*$ keeping the outputs of N in $\mathcal{Y}_a$, and with respect to the best choice of the initial condition $x_{G,0}^*$ of the linear system.

The nonlinearity measure always takes a value between zero and one. $\phi_N^{y_a} = 1$ is only achieved through a linear system producing a zero output and vice versa.

2.1.3 Using Error from Linear Control of Nonlinear Systems

Several research has been carried out in order to decide if a linear controller design is suitable for a given control problem [12, 16, 17, 37]. In a recent work [36], Schweickhardt and Allgower aimed to use a linear model for performance synthesis for the nominal closed loop, while still guaranteeing stability of the closed loop with the nonlinear process. The problem considered is the design of a linear controller C for a nonlinear plant N. The setup of the control system is given in Fig 2.2a. Two exogenous signals are entering the control loop corresponding to what are usually the disturbance signal at the plant input (u_1) and the reference signal (u_2). The regulated variables are the controller output y_2 and the plant output y_1 or their respective inputs e_i. For a controller C for the nominal model, the closed loop can be redrawn as depicted in Fig.2.2b. Here, Δ is

the uncertainty and M the nominal feedback loop, i.e. the interconnection of the linear model G and the controller C.

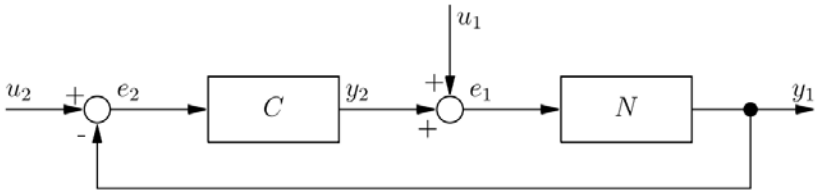

(a) Setup for a linear controller C for the nonlinear plant N

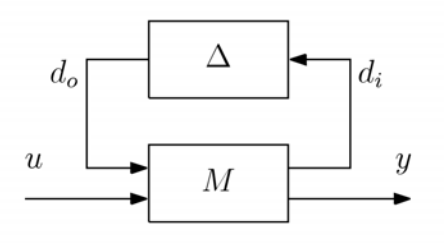

(b) Generalized plant and setup for robust control

Figure 2.2: Designing linear controller for a nonlinear plant [36].

To investigate under which conditions a given nonlinear process N can be represented as the interconnection of G and Δ, *Model Quality Indices* and *Nonlinearity Measures* were defined for 6 different setups as shown in Figure 2.3. The results show that even though principally any linear model can be used, but the best model, with an error gain given by the corresponding nonlinearity measure, was shown to be significantly superior to other models. Also, for a locally stable but globally unstable system it is indeed necessary to do a regional controller design.

Error setup	Model quality index	Nonlinearity measure
Additive error (AE)	$\|\Delta\|^{\mathscr{U}} = \sup_{u\in\mathscr{U},T>0} \frac{\|(Nu-Gu)_T\|}{\|u_T\|}$	$\phi^{\mathscr{U}}_{AE,N} = \inf_{G\in G_{m,n}} \|\Delta\|^{\mathscr{U}}$
Multiplicative output error (MOE)	$\|\Delta\|^{G\mathscr{U}} = \sup_{u\in\mathscr{U},T>0} \frac{\|(Nu-Gu)_T\|}{\|(Gu)_T\|}$	$\phi^{\mathscr{U}}_{\mathrm{MOE},N} = \inf_{G\in G_{m,n}} \|\Delta\|^{G\mathscr{U}}$
Multiplicative input error (MIE)	$\|\Delta\|^{\mathscr{U}} = \sup_{u\in\mathscr{U},T>0} \frac{\|(G^{-1}Nu-u)_T\|}{\|u_T\|}$	$\phi^{\mathscr{U}}_{\mathrm{MIE},N} = \inf_{G\in G_{m,n}} \|\Delta\|^{\mathscr{U}}$
Inverse multiplicative output error (IMOE)	$\|\Delta\|^{N\mathscr{U}} = \sup_{u\in\mathscr{U},T>0} \frac{\|(Nu-Gu)_T\|}{\|(Nu)_T\|}$	$\phi^{\mathscr{U}}_{\mathrm{IMOE},N} = \inf_{G\in G_{m,n}} \|\Delta\|^{N\mathscr{U}}$
Inverse multiplicative input error (IMIE)	$\|\Delta\|^{G^{-1}N\mathscr{U}} = \sup_{u\in\mathscr{U},T>0} \frac{\|(G^{-1}Nu-u)_T\|}{\|(G^{-1}Nu)_T\|}$	$\phi^{\mathscr{U}}_{\mathrm{IMIE},N} = \inf_{G\in G_{m,n}} \|\Delta\|^{G^{-1}N\mathscr{U}}$
Feedback error (FE)	$\|\Delta\|^{N\mathscr{U}} = \sup_{u\in\mathscr{U},T>0} \frac{\|(G^{-1}Nu-u)_T\|}{\|(Nu)_T\|}$	$\phi^{\mathscr{U}}_{FE,N} = \inf_{G\in G_{m,n}} \|\Delta\|^{N\mathscr{U}}$

(a) Definition of model quality indices and nonlinearity measures

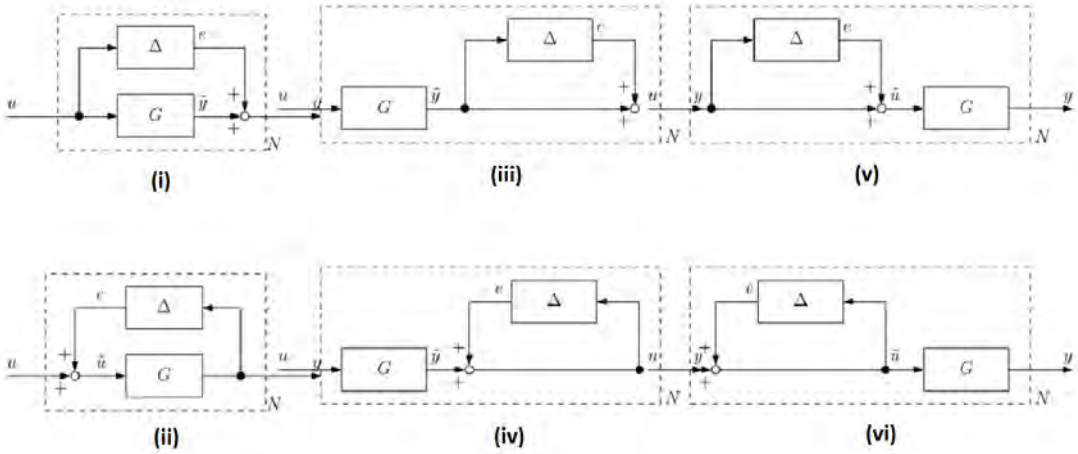

(b) Different possible representations of a general (nonlinear) system N as the interconnection of a nominal (linear) model G and an error system Δ. (i) Additive error; (ii) feedback error; (iii) multiplicative output error; (iv) inverse multiplicative output error; (v) multiplicative input error; (vi) inverse multiplicative input error

Figure 2.3: Different forms of implementation of linear controllers for nonlinear plants [36].

2.2 Data-Based Methods

2.2.1 Linear Cross Correlation

For multiple model bank selection for multi-linear model analysis of a nonlinear process, it is essential to deduce if the system is linear or nonlinear as well as the degree of nonlinearity in the initial stage. A 'Higher Order Spectral' (HOS) based method for determining the total operating space which results in several linear and nonlinear modes was implemented in [19]. 'Linear Cross Correlation Method', which needs less data, is then employed for partitioning a nonlinear mode into a number of linear modes.

For linear time invariant (LTI) systems, the cross-spectral densities associated with the system input/output data can be shown to be sufficient to characterize the system. This analysis uses the second-order moment of the input/output time series. It has been shown that for any LTI system without noise, the squared coherence function (γ_{uy}^2) between the input and the output is equal to one at all frequencies ω [13]:

$$\gamma_{uy}^2(j\omega) = \frac{|\phi_{uy}(j\omega)|^2}{\phi_{uu}(j\omega).\phi_{yy}(j\omega)} = 1 \tag{2.8}$$

Therefore, if the LTI system is driven by a random excitation input signal and there is no measurement noise, the following index is zero [13]:

$$NLI1 = 1 - \max_{\omega} \frac{|\phi_{uy}(j\omega)|^2}{\phi_{uu}(j\omega).\phi_{yy}(j\omega)} \tag{2.9}$$

However, $NLI1$ will be affected by measurement noise.

2.2.2 Amplitude Adjusted Fourier Transformations (AAFT) Surrogates

'Amplitude Adjusted Fourier transformations (AAFT) surrogates' as a statistical method of detecting nonlinearity in univariate short-term time-series of traffic volume was used in [39]. The algorithm is based on [35] and creates AAFT surrogates as proposed by [38], with the alteration that it iteratively refines the amplitudes of the surrogates by a three-step process to avoid the bias towards a slightly flattened spectrum that was observed as a result of the routine's initial form [34].

The underlying concept is: first, a null hypothesis of a linear Gaussian process that creates the time series is established; then, the surrogate data is constructed and, finally, given a selected statistic (e.g., prediction error or time reversibility) its performance is measured upon the real time series in order to reject or accept the primary established hypothesis. An efficient way of reconstructing surrogates is the Fourier Transformation. For a series of volume $\{V_i\}$ of N values taken every t, where $t = t_0, t_1....., t_{N-1}$, discrete Fourier transformation F of the original data is computed as:

$$V(f) = F\{V(t)\} = \sum_{n=0}^{N-1} V(t_n) e^{2\pi i f n \delta t} = A(f) e^{i\phi(f)} \tag{2.10}$$

where $A(f)$ is the amplitude and $\phi(f)$ is the phase. $V(f)$ is calculated in discrete frequency $f = -N\Delta f/2, ..., -\Delta f, 0, \Delta f, ..., N\Delta f/2$, where $\Delta f = 1/(N\Delta t)$. Phases are randomized (rotation of phases in every f by a ω chosen uniformly in the range $[0, 2\pi)$

$$\widetilde{V} = A(f) e^{i[\phi(f)+\varphi(f)]} \tag{2.11}$$

The inverse of the Fourier transformation returns the new series (surrogate) to the time

domain as:

$$\widetilde{V} = F^{-1}\{\widetilde{V}(f)\} = F^{-1}\{V(f)e^{i\varphi(f)}\} \tag{2.12}$$

The resulting series have the same power spectrum and autocorrelation as the original data [29].

In order to generate the best surrogate data, the procedure is repeated several times. The selection of the best surrogate is based on the relative discrepancy to the spectrum at the i^{th} iteration [35]:

$$Relative\ Discrepancy = \frac{\sum_{k=0}^{N-1}(\hat{V}_k^i - \hat{V}_k)^2}{\sum_{k=0}^{N-1}(\hat{V}_k)^2} \tag{2.13}$$

where, $\hat{V}_k^i$ is the smoothed estimate of the spectrum in the i-th iteration. The statistics used in [39] to establish a comparison between the real time series and the constructed surrogate data is the symmetry against time reversal [33]. Time reversibility is a property of stochastic linear processes that presents symmetry in time reversal [5]. Reversibility is calculated by the third-order quantity:

$$\phi^{rev}(\tau) = \frac{\sum_{n=\tau+1}^{N}(V(t_n) - V(t_{n-\tau}))^3}{[\sum_{n=\tau+1}^{N}(V(t_n) - V(t_{n-\tau}))^3]^{\frac{3}{2}}} \tag{2.14}$$

where $V(t_n)$ is a series and τ is the time delay, meaning lagged information on volume [33]. It is found that values of the statistic larger than 3 indicate time irreversibility and, thus, nonlinearity [5].

For the purpose of the analysis, 20 different surrogates were constructed. The test of surrogate data gave satisfactory results regarding its capacity of identifying overall nonlinearity in the traffic volume data.

2.2.3 Other Data Driven Methods

Among the other data driven methods, 'Power Spectrum', 'Bicoherence-based measure', 'Surrogate data-based measure', 'Correlation Dimension' and 'Maximal Lyapunov Exponent' are widely used. They are discussed in the next chapter.

CHAPTER 3

TOOLS FOR DATA-BASED QUANTIFICATION OF NONLINEARITY

The following tools have been employed in this thesis for the purpose of quantification of nonlinearity and comparison of their respective performances.

3.1 Power Spectrum

The power spectrum is a transform of a time series that reveals its frequency content. Its usefulness in detection and diagnosis is that it provides a characterization of the dynamics of a linear or nonlinear time series because each peak in the spectrum indicates a frequency that is present in the time series. The power spectrum can be determined

from the discrete Fourier transform $(X(f))$ of the time series $x(k)$

$$X(f) = DFT(x(k)) = \sum_{k=0}^{N-1} x(k)e^{-j2\pi kf/N} \tag{3.1}$$

where N is the number of samples in the time series. The discrete Fourier transform (DFT) has N frequency channels and is a complex quantity that captures both the amplitude and phase of the frequency components within the time series. The power spectrum considers only the amplitudes and is given by $P(f) = |X(f)|^2$, where f specifies the frequency and $P(f)$ is the spectral power at that frequency. Figure 3.1 is included as

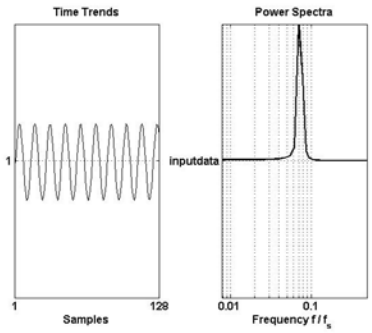

Figure 3.1: The Time Trend and Power Spectrum of a single sinusoid signal.

a reference to show the time trend and the power spectrum of a sinusoid of a single frequency. It shows a single peak indicating that for such sinusoid signals, energy content is at a single frequency only.

3.2 Bicoherence based Method

The bispectrum is the simplest of the various frequency domain Higher Order Statistical (HOS) measures. It is the frequency domain counterpart of the third-order moment and

is defined as

$$B(f_1, f_2) \triangleq E\left[X(f_1)X(f_2)X^*(f_1+f_2)\right] \tag{3.2}$$

where $X(f)$ is the Fourier transform of the continuous time data series $x(t)$. The bispectrum, $B(f_1, f_2)$, at point (f_1, f_2) measures the nonlinear interaction between frequencies f_1 and f_2, [28]. This interaction between frequencies can be related to the nonlinearities present in the signal-generating systems. The bispectrum is normalized in the following way to give a measure called bicoherence whose magnitude is bounded between 0 and 1:

$$bic(f_1, f_2)^2 \triangleq \frac{\left|E\left[X(f_1)X(f_2)X^*(f_1+f_2)\right]\right|^2}{E\left[|X(f_1)X(f_2)|^2\right]E\left[|X(f_1+f_2)|^2\right]} \tag{3.3}$$

where $X(f)$ is the Fourier transform of the data series $x(t)$. Significance of bicoherence magnitude at each individual bifrequency is given by

$$P\{bic(f_1, f_2)^2 > \frac{c_\alpha^{\chi^2}}{2K}\} = \alpha \tag{3.4}$$

where K is the number of data segments used in bicoherence estimation and $c_\alpha^{\chi^2}$ is the critical value calculated from the central χ^2 distribution table for a significance level of α with two degrees of freedom. Those bicoherence values which satisfy the above condition are called $bic^2_{significant}$. The Non-Gaussianity Index (NGI) is given by:

$$NGI \triangleq \frac{\sum bic^2_{significant}}{L} - \frac{c_\alpha^{\chi^2}}{2KL} \tag{3.5}$$

where L is the number of $bic^2_{significant}$. Then,

- if NGI$\leq$0, the signal is GAUSSIAN

- if NGI >0, the signal is NON-GAUSSIAN

The nonlinearity index, defined in [2, 4] is

$$NLI \triangleq \hat{bic}^2_{max} - \left(\overline{\hat{bic}^2_{robust}} + 2\sigma_{\hat{bic}^2,robust}\right) \tag{3.6}$$

where, $\overline{\hat{bic}^2_{robust}}$ and $\sigma_{\hat{bic}^2,robust}$ are, respectively, the robust mean and the robust standard deviation of the estimated squared bicoherence. Then,

- if NLI$\leq$0, the signal is Linear.

- if NLI >0, the signal is Nonlinear.

NLI gives a 'yes' or 'no' answer for the existence of nonlinearity. This index actually measures the flatness of the bicoherence function; it is a useful index when there is no operating point variation (constant steady-state) in the measurement signal. Some researchers such as [19] modified the Bicoherence-based method from [3] and formed the following formulation:

$$NLI2 = \max_{f_1,f_2} bic^2_y(f_1,f_2) - (E[bic^2_y(f_1,f_2)] + 2\sigma[bic^2_y(f_1,f_2)]) \geq T \tag{3.7}$$

where $bic^2_y(f_1,f_2)$ is the bicoherence of $y(t)$ and $\sigma^2 = E[|U(f)|^2]$ and E represents the 'expected value'. The index is further modified as $NLI3$ index that can detect both nonlinearity degree and steady-state changes in input/output data:

$$NLI3 = \max_{f_1,f_2} bic^2_y(f_1,f_{-2}) \geq T \tag{3.8}$$

where T is a given threshold value that should be determined by the practitioner.

Since, NLI gives a qualitatitive 'yes' or 'no' answer for the presence of nonlinearity, it is not very useful for quantification of nonlinearity. Therefore, the 'Total Nonlinearity Index', $TNLI$, as defined in [3], is used for nonlinearity quantification. The $TNLI$ is defined by:

$$TNLI \triangleq \sum bic^2_{significant} \tag{3.9}$$

3.3 Surrogate Data-based Method

Surrogate data is a synthetic data set called surrogate time series, having the same power spectrum but with the phase coupling removed by randomization. A key property of the test time series is then compared to that of its surrogates, and nonlinearity is diagnosed if the property is significantly different in the test time series [21, 38]. For a time-series, the surrogate data is calculated by:

$$\text{z}=FFT(\text{test time series}) \quad ,$$

where, FFT=Forward Discrete Fourier Transform; then,

$$z_{surr} = \begin{cases} z\left[i\right] & i = 1 \\ z\left[i\right] e^{j\phi_{i-1}} & i = 2, ..., N/2 \\ z\left[i\right] & i = N/2+1 \\ z\left[i\right] e^{-j\phi_{N-i+1}} & i = (N/2+2), ...N \end{cases} \tag{3.10}$$

N = number of samples in the time-series. The quantity $\phi_k, k = 1, ..., (N/2-1)$, is a random phase in the range $[0, 2\pi]$.

Then, surrogate data = IFFT(z_{surr}) , where IFFT=Inverse Discrete Fourier Transform.

Steps for calculating Surrogate Data based Nonlinearity N_{surr} are enumerated below:

Step 1 An Embedded matrix is formed for the test data $y(1).....y(l)$

$$\mathbf{Y} = \begin{Bmatrix} y(1) & y(2) & ... & y(E) \\ y(2) & y(3) & ... & y(E+1) \\ y(3) & y(4) & ... & y(E+2) \\ ... & ... & ... & ... \\ y(l-E+1) & y(l-E+2) & ... & y(l) \end{Bmatrix} \tag{3.11}$$

Step 2 For each row $\underline{\mathbf{y_i}}$ of $\mathbf{Y}$ indexes are found such that j_p $(p = 1.....k)$ of k nearest neighbors rows $\underline{\mathbf{y_{jp}}}$ having the k smallest values of $\left|\left|\underline{\mathbf{y_{jp}}} - \underline{\mathbf{y_i}}\right|\right|$ subject to a near-in-time neighbour exclusion constraint $|j_p - i| > E/2$

Step 3 Sum of squared prediction errors for the test data is calculated by:

$$\Gamma_{test} = \sum_{i=1}^{l-H} \left(y(i+H) - \frac{1}{k} \sum_{p=1}^{k} y(j_p + H) \right)^2 \tag{3.12}$$

where H is Prediction Horizon, k is number of near neighbors.

Step 4 M surrogate prediction errors Γ_{surr} by applying Steps 1 through 3 to M surrogate data sets.

Step 5 An embedded matrix is created of both test and surrogate data. Squared Prediction errors of both test data, Γ_{test} and of surrogate data, Γ_{surr} are calculated as described in [3]. Surrogate Nonlinearity Index, N_{surr} is then calculated from :

$$N_{surr} = \frac{\bar{\Gamma_{surr}} - \Gamma_{test}}{3\sigma_{\Gamma_{surr}}} \tag{3.13}$$

where $\bar{\Gamma_{surr}}$ and $\sigma_{\Gamma_{surr}}$ are mean and variances of M sets of Γ_{surr} , respectively.

The recommended default values for the parameters of the nonlinearity detection algorithm are taken from [3].

3.4 Maximal Lyapunov Exponent Method

'Maximal Lyapunov Exponent Method' quantifies nonlinearity of a time series by measuring the extent of 'chaos' in the nonlinear time series. In a nonlinear chaotic time series, several segments of the time series, which are initially very close, gets separated over the course of time and finally become uncorrelated. Difference between 'Stochastic' and 'Chaotic series' is that 'stochastic series' is random at all times and distances whereas 'chaotic series' is predictable in the very short term, but appears random for longer periods. Thus, in a chaotic nonlinear time series, it is impossible to predict the position of the trajectory more than, x time steps ahead, by knowing the position of another trajectory at the current time, which was very close initially. For a dynamical system to display chaotic behavior, it has to be either nonlinear or infinite-dimensional (i.e. 'distributed parameter system'(s) or systems described by partial differential equations). Since all the simulation models used in this thesis are modeled by ordinary differential equations, presence of chaos means that the system is nonlinear.

If the increase in separation of trajectories is exponentially fast, the properly averaged exponent of this increase is characteristic for the system underlying the data and quantifies the strength of chaos. It is called the Lyapunov exponent. In brief, it is a

quantity that characterizes the rate of separation of infinitesimally close trajectories.

Quantitatively, two trajectories in phase space with initial separation δZ_0 and final separation of δZ after a certain time, diverge at a rate given by

$$|\delta Z(t)| = e^{\lambda t}|\delta Z_0| \tag{3.14}$$

where λ is the Lyapunov exponent.

Let s_{n1} and s_{n2} be two points in state space with distance $||s_{n1} - s_{n2}|| = \delta_0 << 1$. Let $\delta_{\Delta n}$ be the distance after time Δn between the two trajectories emerging from these points, $\delta_{\Delta n} = ||s_{n1+\Delta n} - s_{n2+\Delta n}||$. Then, λ is calculated by

$$\delta_{\Delta n} \simeq \delta_0 e^{\lambda \Delta n}, \quad \delta_0 \ll 1, \quad \Delta n \gg 1 \tag{3.15}$$

It determines a notion of predictability for a dynamical system. For the chaotic system it has to be between 0 and 1. To be chaotic, the largest Lyapunov exponent must be between zero and one. If Lyapunov exponent is greater than one, the system is stochastic.

In order to obtain the average exponential growth of distances, the following has to be done [20, 32]:

A point, s_{n0} is chosen of the time series in embedding space and all neighbors with distance smaller than ϵ are selected. Then, the average over the distances of all neighbors to the reference part of the trajectory is computed as a function of the relative time. The logarithm of the average distance at time $\triangle n$ is some effective expansion rate over the time span, $\triangle n$, (plus the logarithm of the initial distance) containing all the deterministic fluctuations due to projection and dynamics. Repeating this for very many values of n_0, the fluctuations of the effective expansion rates will average out. Thus, the

formula is:

$$S(\triangle n) = \frac{1}{N}\sum_{n_0=1}^{N}\left(\frac{1}{|\vartheta(s_{n0})|}\sum_{s_n\in\vartheta(s_{n_0})}|s_{n_0+\triangle n} - s_{n+\triangle n}|\right) \tag{3.16}$$

The reference points s_{n_0} are embedding vectors. $\vartheta(s_{n_0})$ is the neighborhood of s_{n_0} with diameter ϵ. Since it might not be possible to know the minimal embedding dimension, m or the optimal distance ϵ, it is advisable to compute $S(\triangle n)$ for a variety of both values.

The program $lyap\_k$ in the $TISEAN$ package is used to perform the necessary calculations to create the curves $S(\triangle n)$. TISEAN is a software project for the analysis of time series with methods based on the theory of nonlinear deterministic dynamical systems, or chaos theory. Its distribution is in source form (in C and FORTRAN) including full documentation [14]. The executables used in this thesis has been downloaded from http://www.mpipks-dresden.mpg.de/t̃isean/Tisean_3.0.1/index.html.

If for some range of $\triangle n$, the function $S(\triangle n)$ exhibits a robust linear increase, its slope is an estimate of the maximal Lyapunov exponent, λ.

Figure 3.2 shows a sample plot for calculating Maximal Lyapunov Exponent of a data set. The exponential form of the entity on the left hand side of eq 3.16 (i.e. exp(S)) is plotted against time Δn. The encircled portion of the plot shows a robust linear increase of $exp(\Delta S)$ for multiple vales in Δn. The linear region is encircled. The bold green line shows the approximate slope of the linear region of the curves. Each curve corresponds to each value of the embedding dimension. The slope of the linear portion

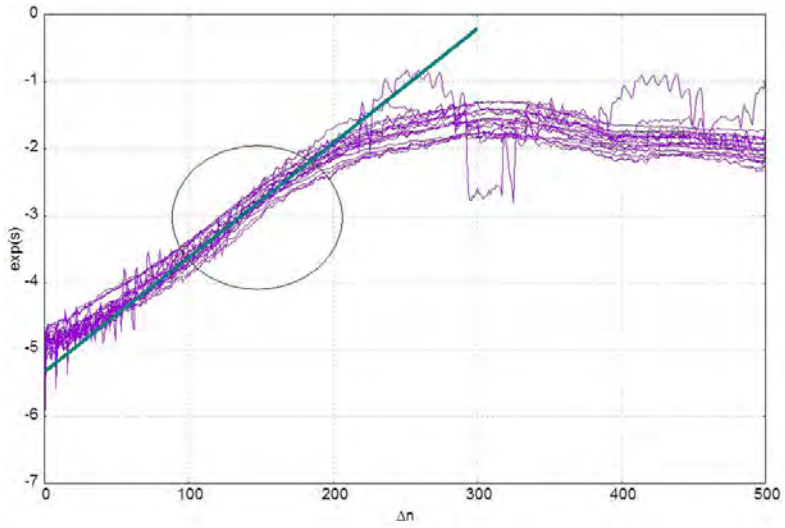

Figure 3.2: Sample plot of $exp(S)$ against Δn for a range of values for embedding dimension.

is approximately 0.015. Thus, Maximal Lyapunov Exponent of the data set is taken to be 0.015, indicating a chaotic nonlinear time series.

3.5 Correlation Dimension Method

Correlation Dimension gives the dimensionality of the space occupied by a set of random points. It is a measure of the extent to which the presence of a data point affects the position of the other point lying on the attractor. An attractor is a set of numerical properties toward which a system tends to evolve, for a wide variety of starting conditions of the system. If correlation dimensions value is finite low and non-integer, the system is chaotic. If correlation exponent increases without bound with increase in the embedding dimensions, the system is stochastic.

The correlation sum for a collection of points x_n in some vector space is the fraction of all possible pairs of points which are closer than a given distance ϵ in a particular norm and is given by:

$$C(m,\epsilon) = \frac{2}{(N-n_{min})(N-n_{min}-1)} \sum_{i=1}^{N} \sum_{j=i+n_{min}}^{N} \Theta(\epsilon - \parallel x_i - x_j \parallel) \tag{3.17}$$

where Θ is the Heaviside step function, $\Theta(x) = 0$ if $x \leq 0$ and $\Theta(x) = 1$ for $x > 0$. The sum just counts the pairs (x_i, x_j) whose distance is smaller than ϵ. In the limit of an infinite amount of data $(N \to \inf)$ and for small ϵ , it is expected that C will vary like a power law, $C(\epsilon) \propto \epsilon^D$, and the local slopes of the correlation sum $d(\epsilon)$ and correlation dimension D are defined by:

$$d(\epsilon) = \frac{\delta ln C(\epsilon, N)}{\delta ln \epsilon} \tag{3.18}$$

$$D = \lim_{\epsilon \to 0} \lim_{N \to \infty} d(\epsilon) \tag{3.19}$$

To find the Correlation Dimension, local slopes of the correlation sum are plotted against ϵ for a range of values of embedding dimension and the value on the y-axis corresponding to the region of the plot where the contour lines become flat is taken as the measure for Correlation Dimension.

For example, Figure 3.3 shows an ideal plot of the local slopes of Correlation Integral against ϵ for calculating Correlation Dimension of a sample data set, provided in the Webpage of $TISEAN$. The flat region is marked with the green line. Again, each curve corresponds to each value of the embedding dimension. The onset of the plateau is at $d(\epsilon) = 2.05$ (marked with a green line). Thus, the value of Correlation Dimension is chosen to be 2.05.

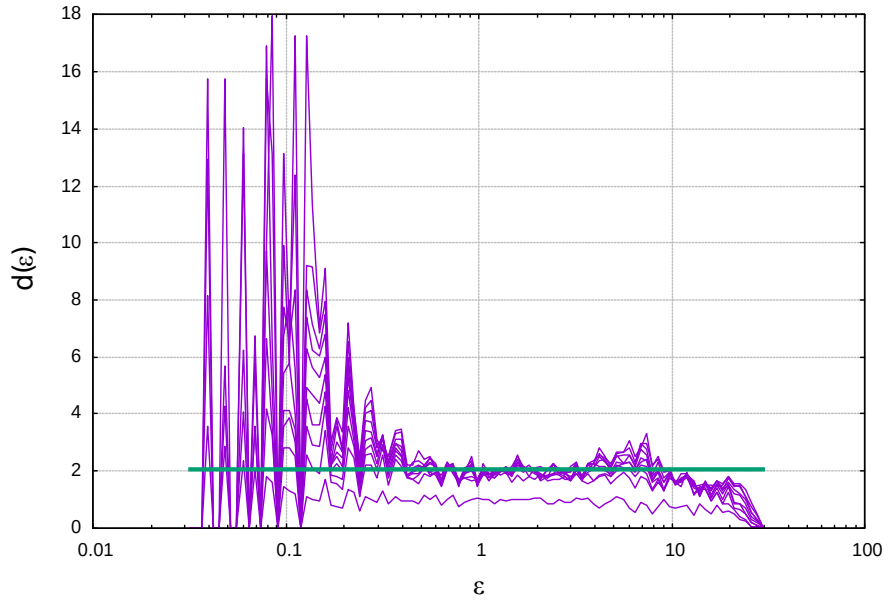

Figure 3.3: Sample plot of local slopes of Correlation Integral against ϵ.

3.5.1 Temporal Correlations

Pairs of points which are measured within a short time span tend to be close in phase space as well and thus introduce a bias when estimating correlation sum. By knowing the typical time over which the data items are correlated, pairs close in that time are rejected.

This problem has been solved by [31] by introducing the space time separation plot. The idea is that in the presence of temporal correlations the probability that a given pair of points has a distance smaller than ϵ does not only depend on ϵ but also on the time that has elapsed between the two measurements. This dependence can be detected by plotting the number of pairs as a function of two variables, the time separation Δt and the spatial distance ϵ. Temporal correlations are present as long as the contour curves

do not saturate and the point of saturation is taken to be the size of the Theiler window. If the signal is periodic from the very start, then half of one period is taken as the size of the Theiler window.

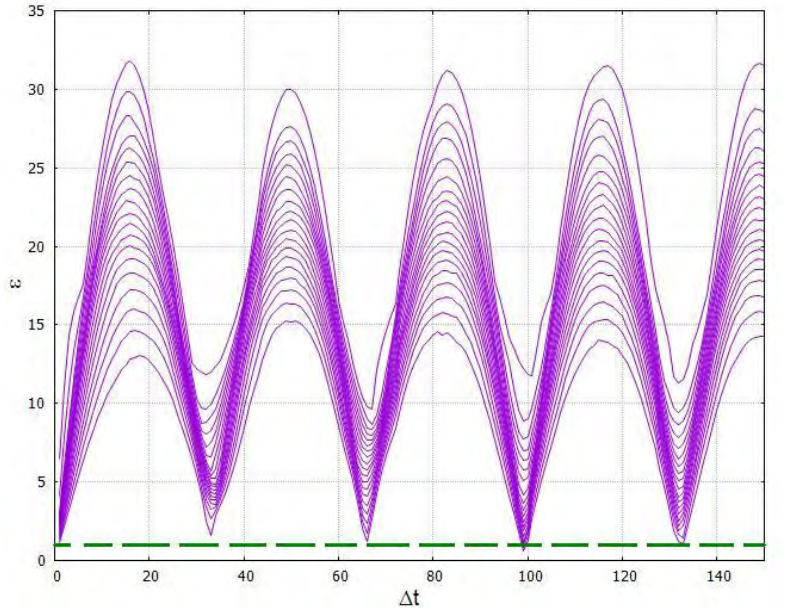

Figure 3.4: Example of a sample stp plot.

Figure 3.4 shows an example of an stp plot of a time series 'amplitude.dat', available in the webpage of $TISEAN$ (The green dashed line marks the onset of the graph for purpose of reference). Since the signal is periodic, half of the period of oscillation can be taken as the Theiler window. Thus, Theiler window can be taken $\backsimeq 20$ but it is suitably chosen much larger, since typically not much statistics is lost, as long as it remains smaller than about 10% of the data set size [14].

3.6 Reconstruction of Phase Space

Calculation of Maximal Lyapunov Exponent and Correlation Dimension are motivated and based on the theory of dynamical systems, which implies that the time evolution is defined in some phase space. Since nonlinear systems can exhibit deterministic chaos, reconstructing phase space is a natural starting point when irregularity is present in the signal. A further assumption made is that the stochastic component is small and essentially does not change the nonlinear properties.

For a purely deterministic system whose present state is fixed, the states at all future times are determined as well. Thus establishing a vector space (called a state space or phase space) is imperative for the system such that specifying a point in this space specifies the state of the system, and vice versa. Then the dynamics of the system can be studied by studying the dynamics of the corresponding phase space points. The concept of the *state of a system* is powerful even for chaotic systems too.

Phase space is an abstract mathematical space spanned by the dynamical variables of the system. The state of the dynamical system at a given instant in time can be represented by a point in this phase space. If there are n dynamical variables, then the state at a given time can be represented by a point in the Euclidean space $\Re^n$. As the dynamical variables change their values in time, the representative point traces out a path in the phase space: a continuous curve in the case of a continuous dynamical system and a sequence of points in the case of a discrete dynamical system.

For reconstructing phase space, two quantities are required: the embedding dimen-

sion, m and the delay, τ such that the time series Y_t can be expressed as:

$$Y_t = \{x_t, x_{t+\tau}, x_{t+2\tau,.....x_{t+(m-1)\tau}}\} \tag{3.20}$$

3.6.1 Time Delay

As seen from Eq 3.20, Time Delay, τ, is defined as the time difference between adjacent components of the delay vectors. It can be calculated by two methods.
The first method involves finding autocorrelation function of the data and selecting τ as its first zero crossing. The second method of determining τ is plotting the time delayed mutual information as described in [10] and determining the first minimum. The second method possesses the advantage of taking the nonlinear dynamical correlations into account whereas the first method is based on linear statistics.

For all the data-series generated and tested for nonlinearity in this thesis, both methods for calculating τ have been applied and similar results were observed. So only the results from the 'Autocorrelation Function' have been documented.

3.6.2 Embedding Dimension

The embedding dimension, m, is an important parameter for the analysis of time series from the dynamical system approach, and determines the dimension of the Euclidean pseudo-space in which supposedly the attractor is reconstructed from the time series. m should be minimum but sufficiently large to unfold the attractor and is usually estimated by calculating the "false nearest neighbors". This method increases the embedding dimension by one at each step and counts the percentage of points for which its nearest

neighbor falls apart with the addition of a new component (from embedding dimension m to $m+1$), and therefore these points are called false nearest neighbors. The estimated minimum embedding dimension is the one that first gives an insignificant percentage of false nearest neighbors.

Calculation of False Nearest Neighbors is carried out using the $false\_nearest$ executable in the $TISEAN$ package. The method searches for points in the data set which are neighbors in embedding space, but which should not be neighbors since their future temporal evolution is too different. For each point of the time series, its closest neighbor in m dimensions is taken into account, and the ratio of the distances between these two points is computed in both $m+1$ and m dimensions. If this ratio is larger than a threshold, the neighbor was false. This threshold, however, has to be large enough to allow for exponential divergence due to deterministic chaos.

A typical example from the output file the *flase_nearest* executable is given in Table 3.1. In this example, it is seen that for embedding dimensions, greater than 4, the fraction of false nearest neighbors becomes zero. Thus 'm'=4 is chosen as embedding dimension for the concerned data set.

3.7 Auto-Correlation Plot

The 'Autocorrelation Function' (ACF) measures the linear predictability of the series at time t, say x_t using only the value x_s. ACF is bounded between -1 and $+1$ where the upper and lower limit represents perfectly positive correlation and perfectly negative correlation respectively; a value of ACF close to 0 depicts minimal if not zero correlation.

Embedding Dimension	Fraction of False Nearest Neighbors
1	0.974
2	0.207
3	0.00279
4	0.00405
5	0
6	0

Table 3.1: Example of output from the file generated by $false\_nearest$

It is calculated by:

$$C(\tau) = \frac{1}{N-\tau} \frac{\sum_{s=1}^{N}(x_s - \bar{x})(x_{(s+\tau)} - \bar{x})}{\sigma^2(x)} \tag{3.21}$$

where τ is the time delay, σ is the standard deviation and $\bar{x}$ is the average of the data.

CHAPTER 4

NONLINEARITY ANALYSIS OF ANALYTICAL TIME SERIES

Often process contains nonlinearities that can be presented by nonlinear functions such as exponential, logarithmic and square functions. White noise and/or similar disturbances always enter processes and may propagate through the interconnected equipment by measurements, feedback and other control actions. This chapter consists of two sections. The first section attempts to quantify nonlinearity of such nonlinear functions from the output time series data. The second section discusses an example of a time series of varying nonlinearity, which has been used for evaluation of nonlinearity measures.

4.1 Analysis of Output Time Series Data of Nonlinear Functions

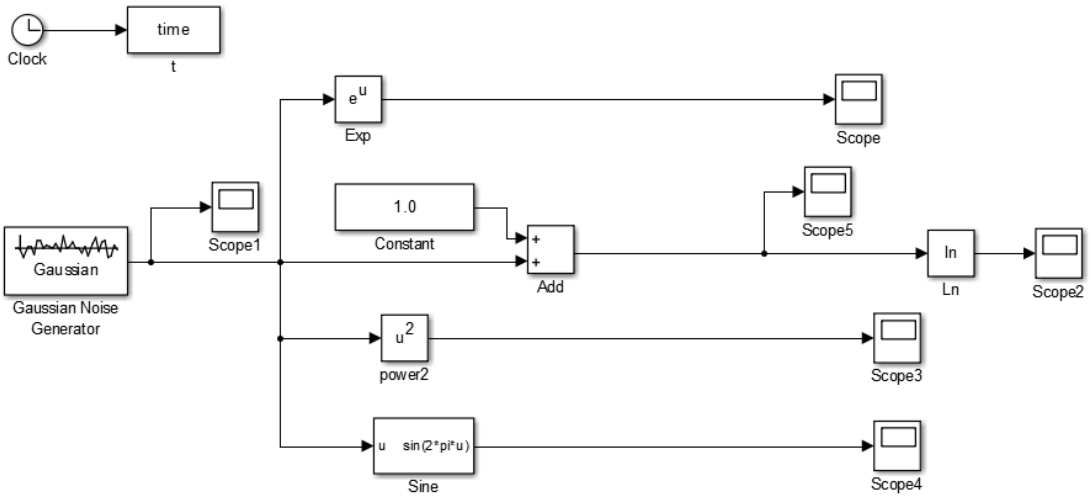

Figure 4.1: Simulink Model for generating Time Series data from Mathematical Functions

Figure 4.1 shows a Simulink block diagram for generating nonlinear time series signals. White noise is passed through respective functions of Exponential (exp), natural logarithmic (ln), square (referred to as 'power 2') and sinusoids (sin). The generated data are tested for nonlinearity quantification.

4.1.1 Time Series Data

Figure 4.2 shows the time series trend and the power spectrum of the output data from these nonlinear functions. The figure also contains the time trend and the power spectrum of the input data (tagged 1). Every output time series from the nonlinear functions

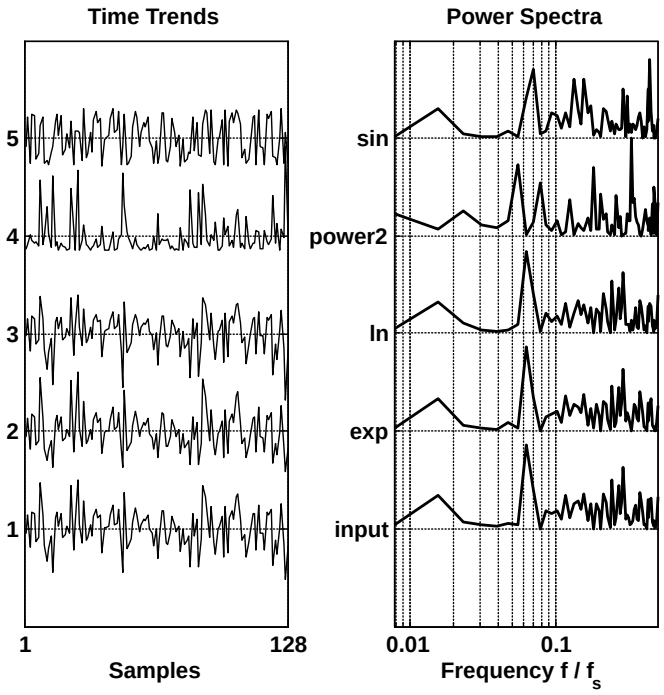

Figure 4.2: Time trends and Power Spectrum of exponential (exp), logarithmic (ln), squared (power2), sinusoidal (sin) functions driven by white noise

shows peaks in additional frequencies than those in the power spectrum of the 'input data'. This portrays the nonlinearity of each the output time series.

4.1.2 Nonlinearity Analysis

4.1.2.1 Results with Bicoherence-based measure

The Total Nonlinearity Index described in Section 3.2 has been computed for all time series data obtained by driving the nonlinear functions with white noise. The results are tabulated in Table 4.1. Table 4.1 indicates that Bicoherence-based measure failed to capture nonlinearity of exponential and sinusoidal functions when driven by white

Function	TNLI
Exponential	0.00
Logarithmic	0.10
Squared (Power of 2)	32.60
Sinusoidal	0.00

Table 4.1: TNLI results for Nonlinear functions driven by white noise

noise. The highest nonlinearity is obtained for 'Squared' function. The output series from logarithmic function is also shown to contain nonlinearity but not as high as that from the square function.

4.1.2.2 Results with Surrogate-Data Method

The 'Surrogate Nonlinearity Index', described in Section 3.3, has been computed for all time series data obtained by driving the nonlinear functions with white noise. The results are tabulated in Table 4.2. It is seen that Surrogate data-based measure was not able to capture nonlinearity of logarithmic and squared functions when driven by white noise. The exponential and sinusoidal functions exhibit moderate nonlinearity.

4.1.2.3 Calculation of Maximal Lyapunov Exponent

Before Calculating Maximal Lyapunov Exponent and Correlation Dimension, evaluation of a few parameters such as 'Time Delay', 'Embedding Dimension' and 'Theiler Window' are required. These parameters are evaluated first in the following subsections.

Function	N_{surr}
Exponential	0.34
Logarithmic	-0.013
Squared (Power of 2)	-0.32
Sinusoidal	0.37

Table 4.2: N_{surr} results on mathematical functions driven by white noise

4.1.2.3.1 Calculation of Time-Delay (τ)

Figure 4.3 shows the Auto-correlation plots of the output time series data from the functions. It is observed that the first zero-crossing of almost all the functions is approximately equal to 1. Thus, the value of time-delay, τ is chosen to be 1 for all the functions.

4.1.2.3.2 Calculation of Embedding Dimension (m)

The method for finding embedding dimension employs calculation of false nearest neighbors. The 'False_nearest' code from $TISEAN$ package is used for this purpose. The output from the codes are recorded in a '.text' file by default. The results from the output text file for the 'Squared' function is given below:

Referring to the tutorial example of Table 3.1 in Chapter 3, the embedding dimension is chosen to be the dimension at which 'the fraction of false nearest neighbors' becomes insignificant and continues to stay as such for dimensions larger than that.

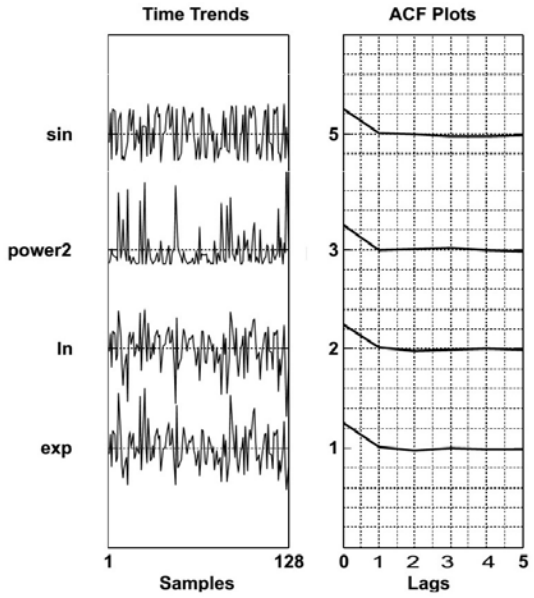

Figure 4.3: Time trends and Autocorrelation Plots of exponential (exp), logarithmic (ln), squared (power2), sinusoidal (sin) functions driven by white noise.

The results from the 'Squared Function' are presented in Table 4.3. As observed, for the squared function, all embedding dimensions higher than 11 gives null value for fraction of false nearest neighborhood. Thus $m = 11$ is chosen for this particular time series data.

The embedding dimensions for the other functions are calculated using the same method. The results are summarized in Table 4.4

4.1.2.3.3 Determination of Theiler Window

To remove temporal correlations from our calculations, determination of Theiler window is required. The feat is accomplished by plotting pairs of data points against both

dimension	fraction of false nearest neighbors
1	0.996
2	0.991
3	0.861
4	0.667
5	0.533
6	0.464
7	0.407
8	0.366
9	0.301
10	0.250
11	0.344
12	0.00
13	0.00

Table 4.3: Results for Squared function driven by white noise

spatial separation, ϵ, and time of separation, Δt. The resulting plot is called Space-time Separation (stp) plot of the data. Figure 4.4 shows the space-time separation (stp) plots of the output time series from the four nonlinear functions. Each of the multiple curves in each plot refer to a different value of embedding dimension. All the plots show a

Function	Embedding Dimension
Exponential	7
Logarithmic	7
Power of 2	11
Sinusoidal	8

Table 4.4: Embedding Dimensions chosen for nonlinear mathematical Functions

stop in steady increasing after $\triangle t$ of 20. Thus, as per conditions stated in Section 3.5.1, $\Delta t = 20$ is a logical choice for Theiler window for the time series data, involved.

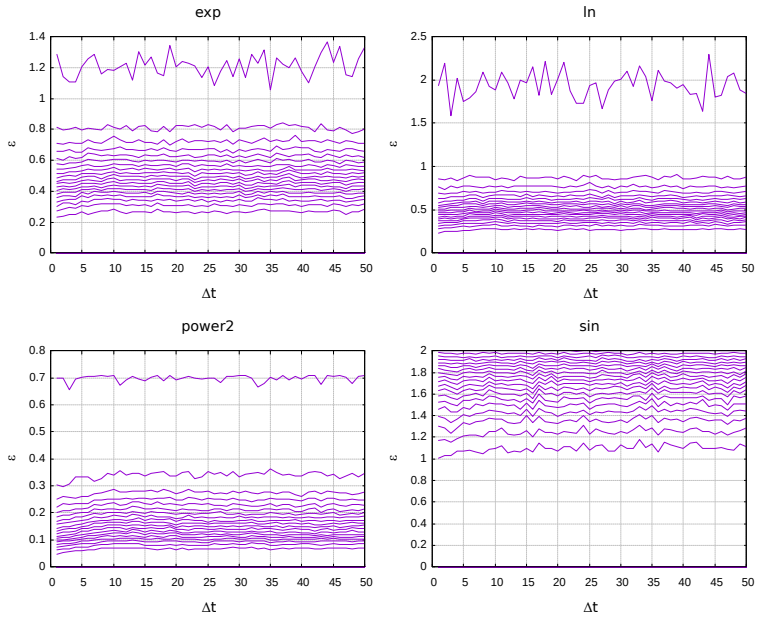

Figure 4.4: Space-time Separation plots of exponential (top left), Logarithmic (Top right), Sinusoidal (bottom right) and Squared (bottom left) functions, driven by white noise

4.1.2.3.4 Results with Maximal Lyapunov Exponent

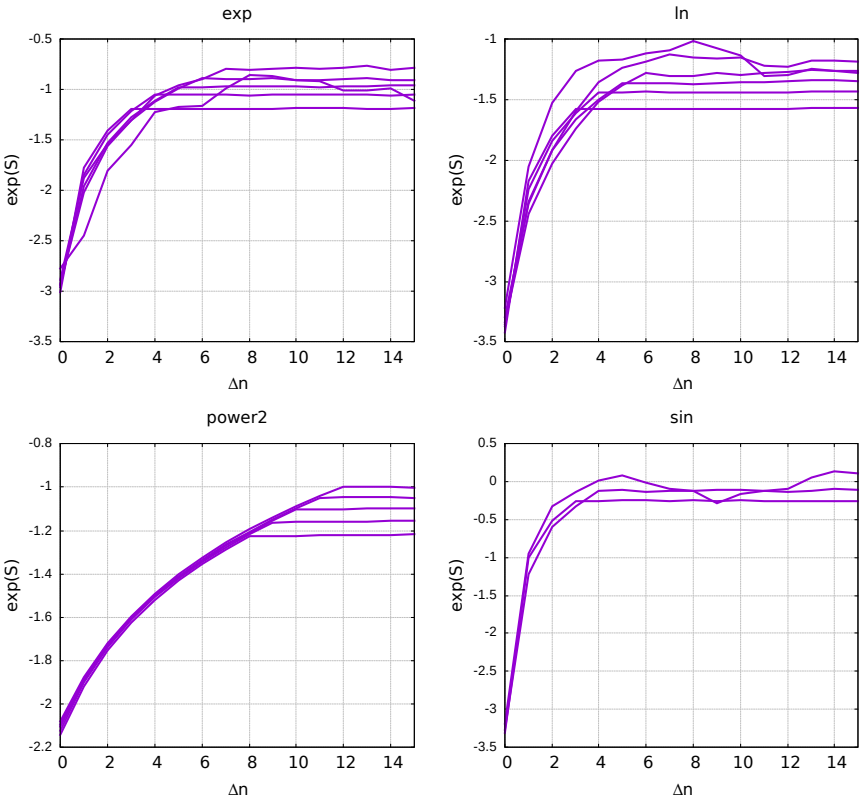

Figure 4.5: Estimation of Maximal Lyapunov Exponenets of exponential (top left), Logarithmic (Top right), Sinusoidal (bottom right) and Squared (bottom left) functions driven by white noise

As shown in the bottom left panel of Figure 4.5, for the 'square' function, driven by white noise, the linear region has an approximate slope of $0.38/6$ or 0.0633. Thus Maximal Lyapunov Exponent for the squared function is $\lambda_{squared} = 0.38/6 = 0.0633$. Similarly, the Maximal Lyapunov Exponent for the logarithmic and exponential functions are calculated and summarized in Table 4.5. The graph of exponential form of ΔS against

Δn of equation 3.16 are plotted for multiple embedding dimensions (hence the multiple curves in each plot) in Figure 4.5.

It is to be noted that the plots for 'sin' function (bottom right plot in Figure 4.5) shows a steep increase while moving from $\Delta n = 0$ to $\Delta n = 1$. No robust linear increasing region is found on this plot. So Maximal Lyapunov Exponent does not exist for this function.

Function	Maximal Lyapunov Exponent
Exponential	0.258
Logarithmic	0.329
Squared (Power of 2)	0.063
Sinusoidal	n/a

Table 4.5: Maximal Lyapunov Exponents for the four Nonlinear Functions

As shown in Table 4.5, Exponential, Logarithmic and Squared (Power 2) all exhibited a Maximal Lyapunov Exponent between 0 and 1. Thus, Maximal Lyapunov Exponent identifies these time series data to be chaotic and hence, nonlinear (according to the condition, discussed in Section 3.4). The exponential and the logarithmic functions contain more nonlinearity than squared (power of 2) function.

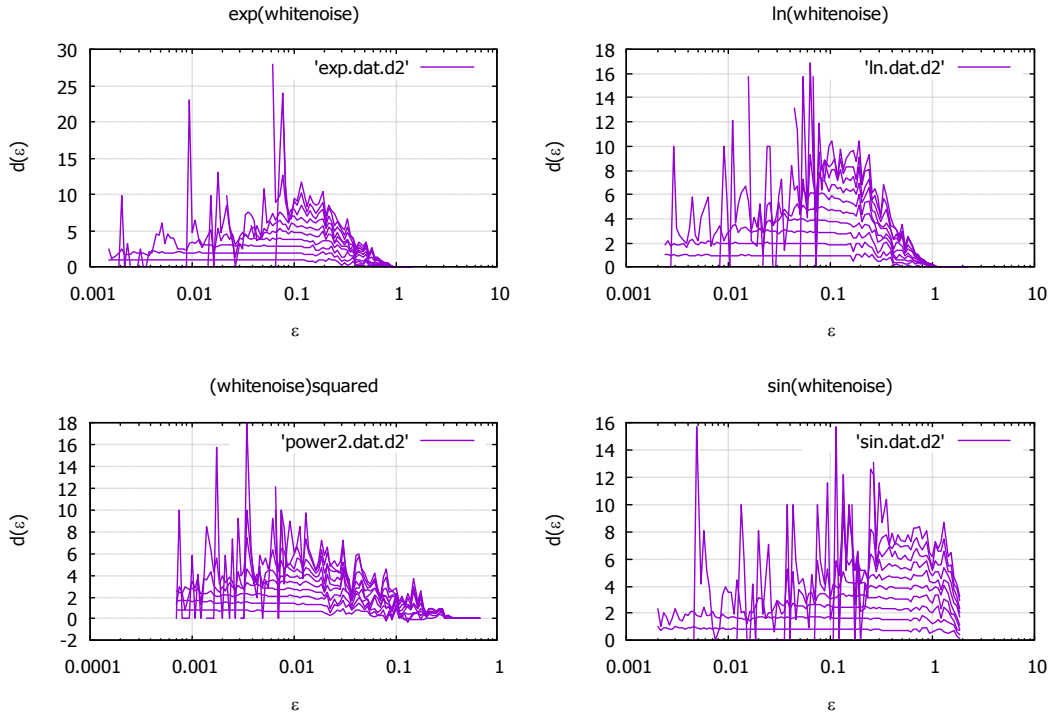

Figure 4.6: Plots of Local Slopes of Correlation Sums against spatial separation for exponential (top left), Logarithmic (Top right), Sinusoidal (bottom right) and Squared (bottom left) functions driven by white noise

4.1.2.4 Results with Correlation Dimension

Figure 4.6 shows the plot of local slopes of Correlation Integrals, $d(\epsilon)$ plotted against spatial distance, ϵ, (Equation 3.18); the plots are made for multiple values of embedding dimensions as portrayed by multiple curves in each plot. The procedure to get the Correlation Dimension from such plots is illustrated in Figure 3.3.

From the three plots except the bottom-right one in Figure 4.6, it is observed that the contours flatten at $y = 0$. Thus Correlation Dimension is 0 for these 3 functions.

From the bottom-right plot in Figure 4.6, it is observed that the sinusoidal function has no flat region (or Plateau) where all the contours converge. So, it does not have any quantifiable Correlation Dimension.

4.1.3 Overall Comparison of the Nonlinearity Measures

Function	TNLI	N_{surr}	Correlation Dimension	Maximal Lyapunov Exponent
Exponential	0.00	0.34	0	0.258
Logarithmic	0.10	-0.013	0	0.329
Squared (Power of 2)	32.60	-0.32	0	0.0633
Sinusoidal	0	0.37	n/a	n/a

Table 4.6: Summary of results of the four Nonlinearity Measures on the Nonlinear Functions

The nonlinearity analysis results have been summarized in Table 4.6. On basis of these results, it can be concluded that Maximal Lyapunov Exponent is a favorable choice for quantification of nonlinearity arising from logarithmic, exponential and squared functions. Bicoherence-based measure is a good method for quantification of nonlinearity arising due to 'squared' functions. Surrogate Nonlinearity Index can be used to quantify nonlinearity arising from exponential and sinusoidal functions. More tests with varying parameters are required for concluding about Correlation Dimension.

4.2 Analysis of Time Series Data of Nonlinear Sinusoidal Signals with Noise

An analytical signal is generated by adding two sinusoids, each having a different frequency and phase. The Simulink model block diagram is shown in Figure 4.7. The

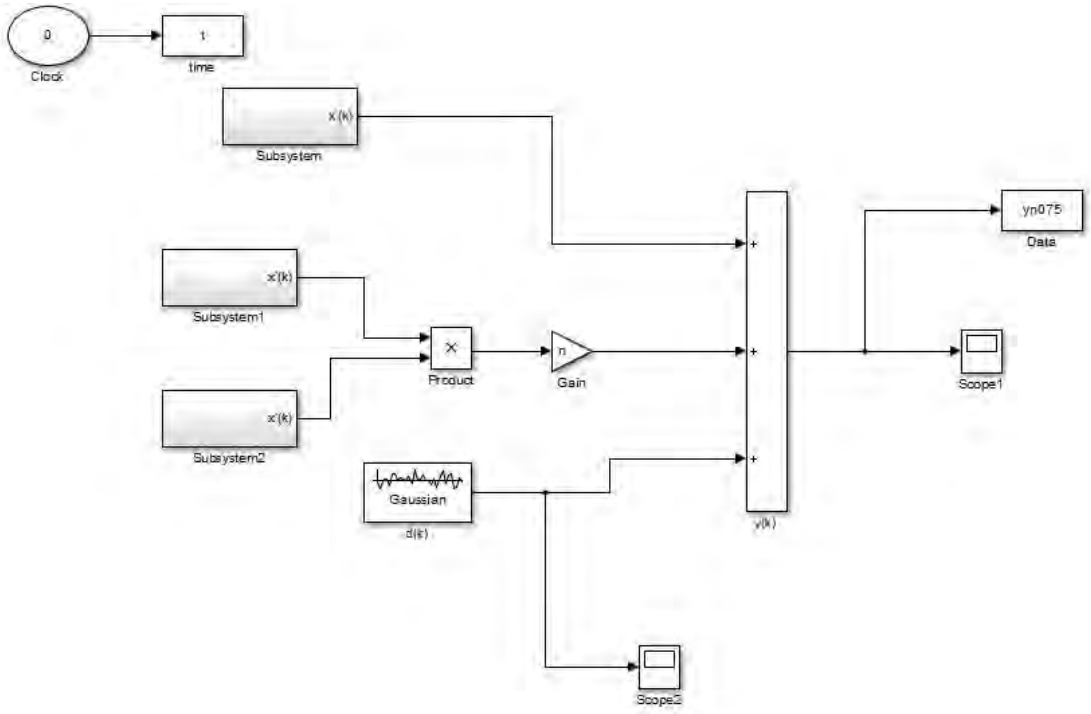

Figure 4.7: Simulink model for Signal Generation

analytical equations for generating this signal, y(k), are as follows:

$$x'(k) = sin(2\pi f_1 k + \phi_1) + sin(2\pi f_2 k + \phi_2) \tag{4.1}$$

$$x(k) = x'(k) + d(k) \tag{4.2}$$

$$y(k) = x'(k) + n_l * x'(k)^2 + d(k) \tag{4.3}$$

where $f_1 = 0.12, f_2 = 0.30, \phi_1 = \pi/3, \phi_2 = \pi/8, n_l$ is a multiplication factor for for nonlinearity contribution and $d(k)$ is white noise sequence with a variance of 0.04. Values of n_l chosen for the experiment are $0(linear), 0.05, 0.25, 0.50, 0.75$ and 1.00.

4.2.1 Time Series Data

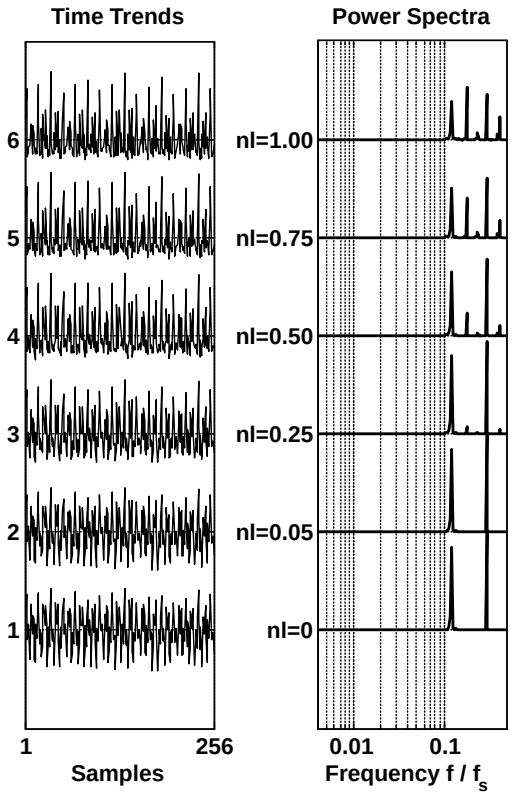

Figure 4.8: Time Trends and Power Spectrum of nonlinear sinusoid signals with increasingly nonlinearity from bottom to top.

Figure 4.8 shows the time series trend and the power spectrum of each generated signal. when $n_l = 0$, there are only two sinusoids and thus the power spectrum shows only two peaks (Tag 1). As value of n_l increases, the number of peaks in the power

spectrum also increases, showing the presence of additional frequencies.

4.2.2 Nonlinearity Analysis

4.2.2.1 Bicoherence Based Results

The Total Nonlinearity Index described in Section 3.2 has been computed for all time series data obtained by combination of sinusoids. The results are tabulated in Table 4.7. As shown in the Table, Bicoherence-based measure gives increasing values of TNLI for

Value of n_l	TNLI
0	0
0.05	5.67
0.25	17.74
0.50	22.95
0.75	25.81
1.00	26.11

Table 4.7: TNLI results for Nonlinear combination of sinusoids

increasing values of n_l. This shows that Bicoherence-based measure, Total Nonlinearity Index (TNLI), is sensitive to the changes in degree of nonlinearity of time series signal.

4.2.2.2 Surrogate Data Based Results

The 'Surrogate Nonlinearity Index', described in Section 3.3 has been computed for all time series data. The results are tabulated in Table 4.8. Surrogate Nonlinearity Index

Value of n_l	N_{surr}
0	0.025
0.05	0.51
0.25	0.64
0.50	0.88
0.75	0.30
1.00	0.35

Table 4.8: N_{surr} results for Nonlinear combination of sinusoids

showed different sequence in rising of nonlinearity in different runs of the algorithm but overall there was an increasing trend in nonlinearity from $n_l = 0$ to $n_l = 1.0$. The tabulated results are from one such run which shows that N_{surr} increases for $n_l = 0$ to $n_l = 0.50$ and then experiences a sudden drop and then increases again. However, in different runs, the drop occurred at different values of n_l. From the behavior of N_{surr}, it can be stated that N_{surr} provides consistent results upto a certain degree of nonlinearity. It may produce erroneous results for very high degree of nonlinearity.

4.2.2.3 Calculation of Maximal Lyapunov Exponent

As stated previously, before Correlation Dimension and Maximal Lyapunov Exponent can be calculated, some additional parameters are to be calculated. They are‘ Time Delay’, ‘Embedding Dimension’ and ‘Theiler Window’.

4.2.2.3.1 Calculation of Time-Delay

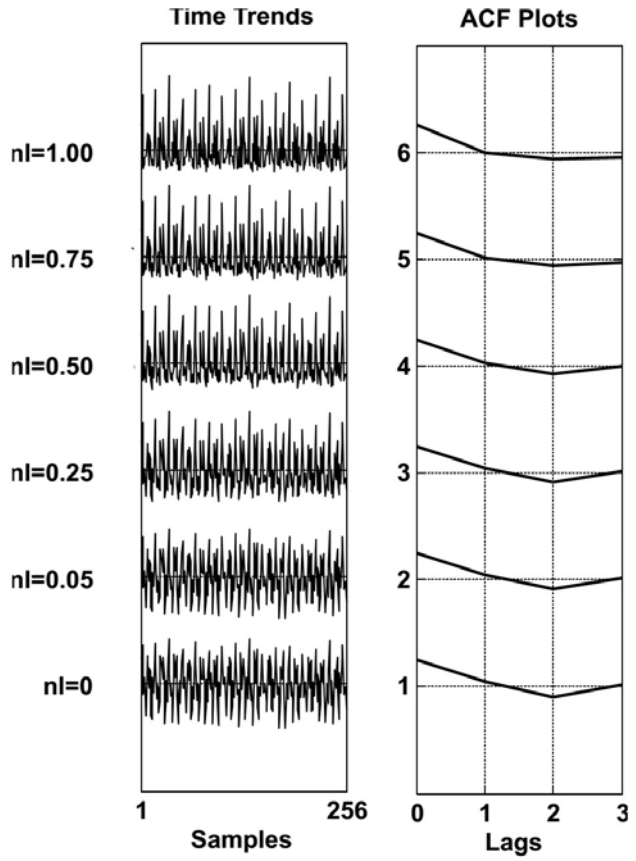

Figure 4.9: Time Trends and Auto-correlation Plots of increasingly nonlinear sinusoid signals.

Figure 4.9 shows that the autocorrelation curves of all four data-sets cross x-axis close to 1. Thus, τ is selected as 1.

4.2.2.3.2 Calculation of Embedding Dimension

A sample calculation of False neighborhoods for $n_l = 0.25$ is shown in Table 4.9 : In

dimension	fraction of false nearest neighbors
1	0.996
2	0.995
3	0.694
4	0.249
5	0.700
6	0.136
7	0.00611
8	0.0212
9	0
10	0
11	0

Table 4.9: Calculation of False neighbourhood for $n_l = 0.25$

accordance to the explanation offered previously, the embedding dimension is chosen

as 8 for $n_l = 0.25$. The values of embedding dimensions for other values of n_l are summarized in Table 4.10.

Value of n_l	Embedding Dimension
0	6
0.05	7
0.25	8
0.50	9
0.75	8
1.00	7

Table 4.10: Embedding Dimensions for values of n_l based on false Nearest Neighbors

4.2.2.3.3 Determination of Theiler Window

The space time separation plots are shown below: In Figure 4.10, all the plots reach a steady oscillatory state fairly early. For the sake of safety, a Theiler window of size $\Delta t = 10$ is used calculating Correlation Dimension.

4.2.2.3.4 Results with Maximal Lyapunov Exponent

The plots of $exp(S)$ against Δn of Equation 3.16 for the all the generated analytical signals are shown in Figure 4.11: None of the plots in Figure 4.11, show any portion

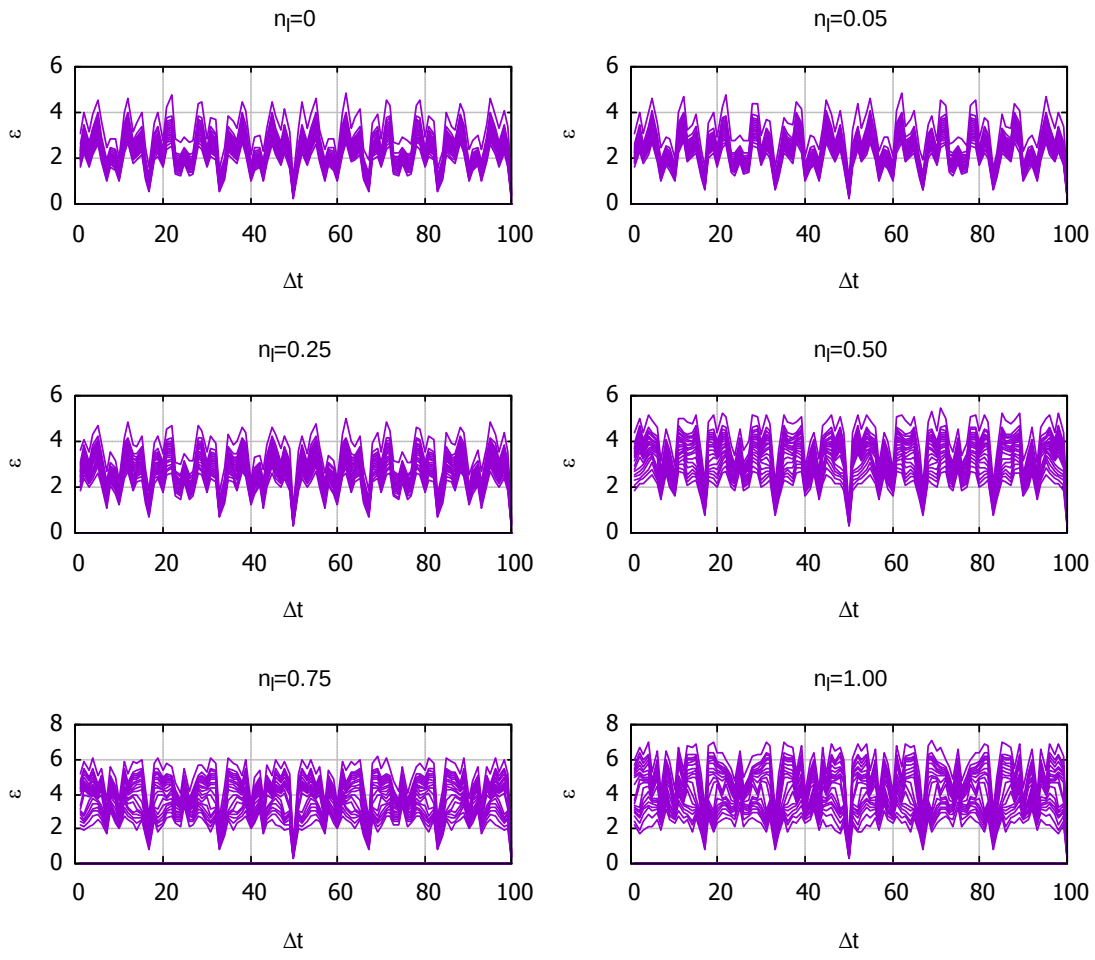

Figure 4.10: Space Time Plots of Nonlinear Sinusoidal Signals

where they are of constant gradient (as compared to the linear portion of the plot in Figure 3.2). Thus, Maximal Lyapunov Exponents cannot be determined for these time series.

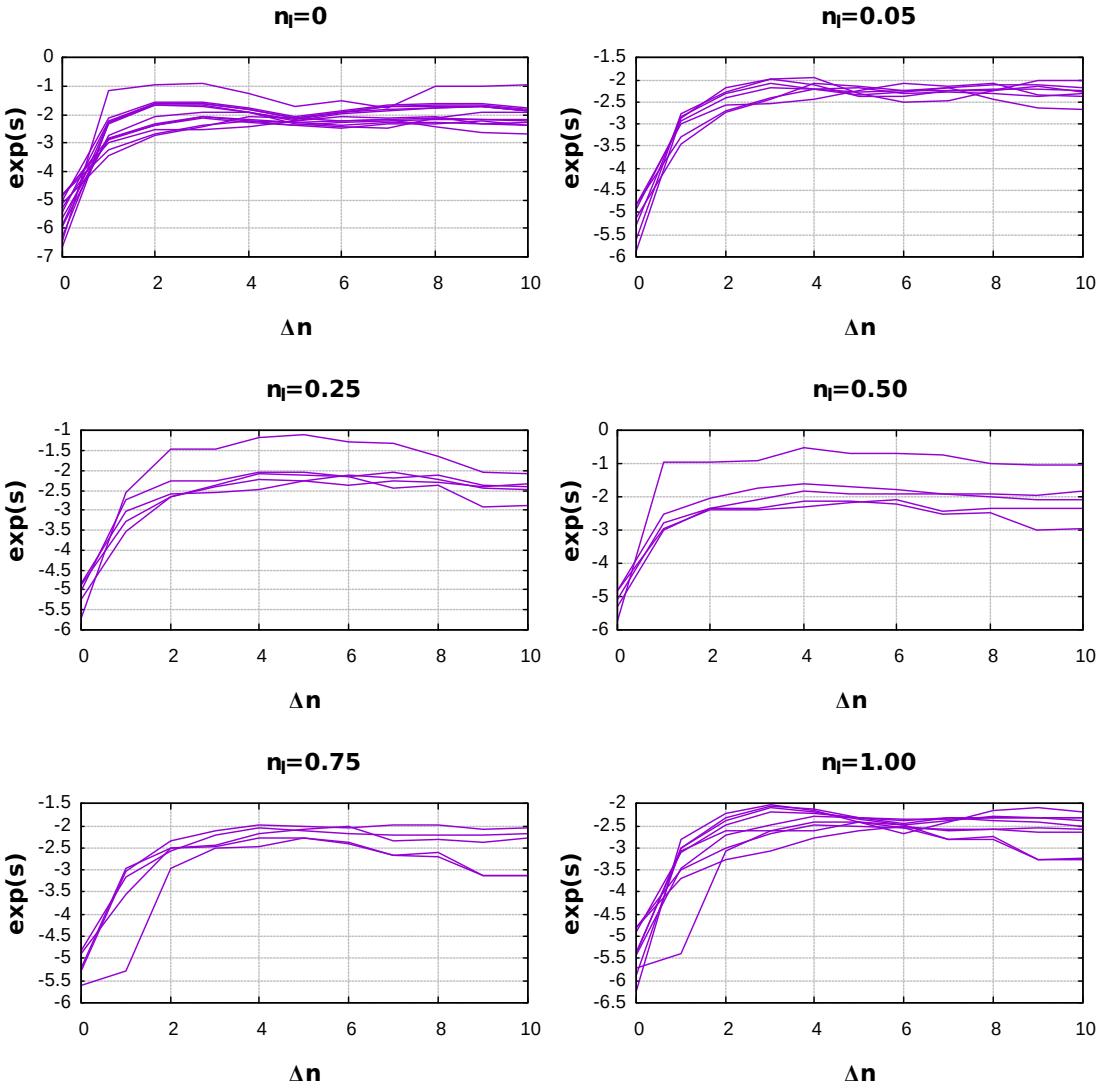

Figure 4.11: Plots of $exp(s)$ against Δn for increasingly nonlinear sinusoids.

4.2.2.4 Correlation Dimension Based Results

The plots of the local slopes of correlation integrals, $d(\epsilon)$, for multiple values of embedding dimension, against spatial separation, ϵ, are shown in the Figure 4.12

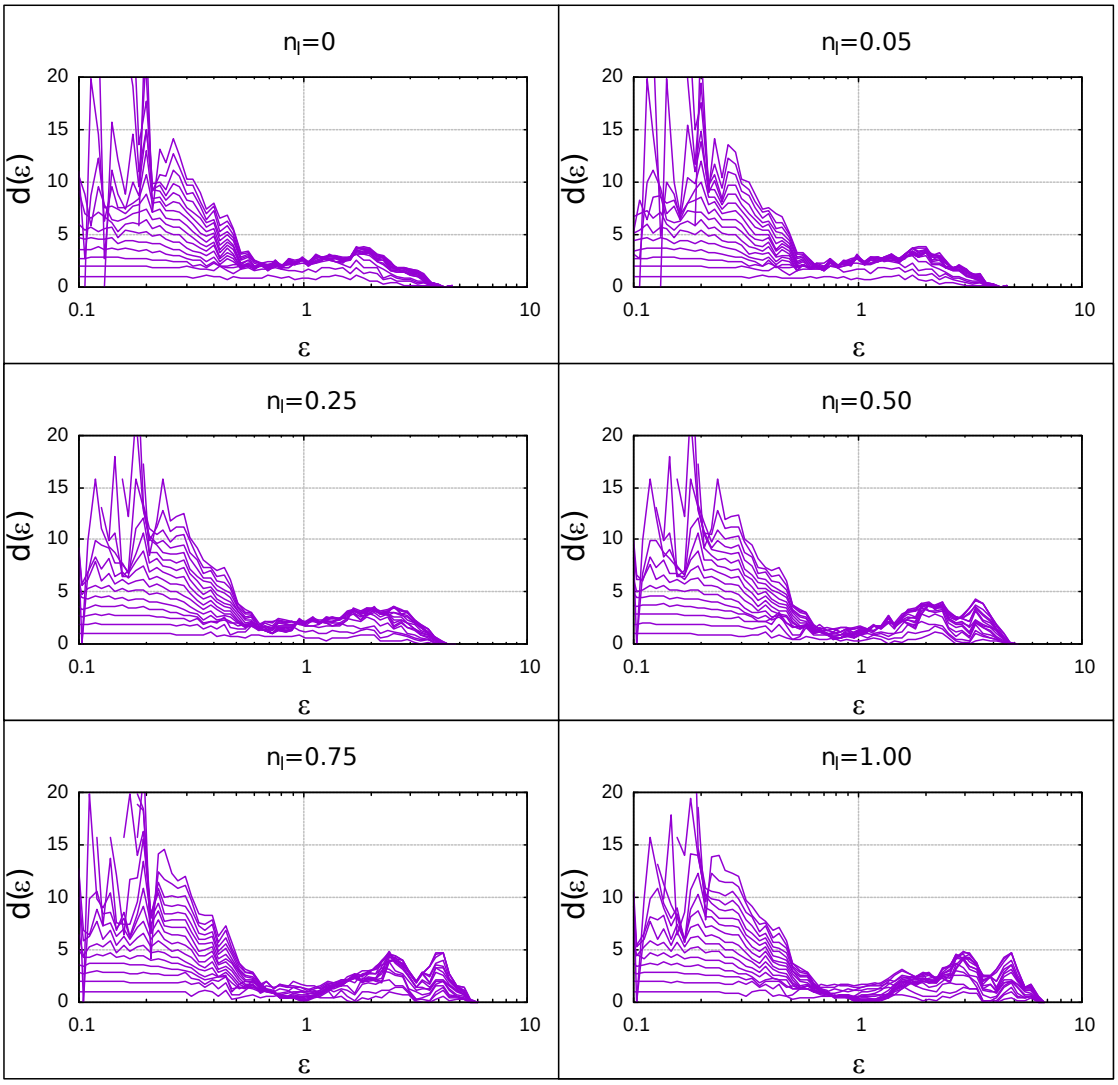

Figure 4.12: Local Slopes of Correlation Integrals against spatial separation for Nonlinear Sinusoidal Signals

All the plots in Figure 4.12 show onset of plateau comparable to the one in example Figure 3.3. Correlation Dimension, C_d shows a decreasing trend with increasing nonlinearity. However, the decrease in C_d is not pronounced as compared to the degree of increase in nonlinearity. The values of C_d are almost the same ($C_d \approx 2.5$) for

$n_l = 0, 0.05, 0.25$. C_d decreased from ≈ 2.5 to ≈ 1.5 when n_l increased from 0.25 to 0.50. Increasing n_l farther to 0.75 renders C_d a positive value very close to 0. When $n_l = 1.00$, C_d is 0. Since Correlation Dimension shows opposite behavior to increase in nonlinearity, it cannot be used to quantify nonlinearity for these data sets.

4.2.3 Overall Comparison

Value of n_l	TNLI	N_{surr}	Correlation Dimension	Maximal Lyapunov Exponent
0	0	0.025	≈ 2.6	n/a
0.05	5.67	0.51	≈ 2.5	n/a
0.25	17.74	0.64	≈ 2.15	n/a
0.50	22.95	0.88	≈ 1.5	n/a
0.75	25.81	0.30	≈ 0.2	n/a
1.00	26.11	0.35	0	n/a

Table 4.11: Summary of results of the four measures on various degree of Nonlinear combination of sinusoids

Even though Bicoherence-based measure did not register any result when applied to a sinusoid of a single frequency (from Table 4.6), it yielded results when applied to a combination of sinusoids. Table 4.11 shows that TNLI increases with increasing values for n_l and thus shows the highest sensitivity to nonlinearity for the concerned time series

data sets.

Even though N_{surr} shows an overall increasing trend with increase in n_l upto a certain degree. However, for very high nonlinearity, it may produce erroneous results as seen for $n_l \geq 0.75$.

Correlation Dimension showed a decreasing trend with increasing values of n_l. Also, the deviation in Correlation Dimension with respect to each change in n_l is small. Since Correlation Dimension shows opposite behavior to increase in nonlinearity, it cannot be quantitatively used to quantify nonlinearity for processes in which, nonlinearity evolves due to combination of sinusoidal signals. However, it can be used qualitatively.

Maximal Lyapunov Exponent could not detect nonlinearity in this kind of signals.

Thus, it can be stated that for a data-set consisting of a combination of sinusoidal signals, Bicoherence-based measure showed the best promise for reliable quantification of nonlinearity.

CHAPTER 5

SIMULATION STUDY FOR NONLINEARITY ANALYSIS

In reality, most processes are nonlinear in nature but they can be operated in a 'locally linear' fashion. The nonlinearity which are locally linear in the presence of small excitations are called *soft nonlinearities*. On the other hand, some nonlinearities are strong and discontinuous in nature; they are called *hard nonlinearities*, for examples, valve stiction, hysterisis and deadband.

This chapter describes some of the nonlinear process systems in the real world. These processes are simulated using MATLAB and SIMULINK and each process is excited sinusoidally. The reason for using a sinusoid signal is because linear systems exhibit *sinusoidal fidelity*, i.e. a sinusoidal input will produce a sinusoidal output of the same frequency but nonlinear systems will produce additional frequencies as well. The output time-series data are then studied for the quantification of nonlinearity.

5.1 Study of a Nonlinear Continuous Stirred Tank Reactor (CSTR)

5.1.1 Process Description

The widely used nonlinear process for simulation study is a nonlinear Continuous Stirred Tank Reactor (CSTR) as shown in Figure 5.1. It is assumed that a single irreversible, exothermic, first-order reaction is taking place in the CSTR. The reaction is $A \rightarrow B$. A perfect mixing in the reactor is assumed i.e. the spatial concentration and temperature differences are ignored.

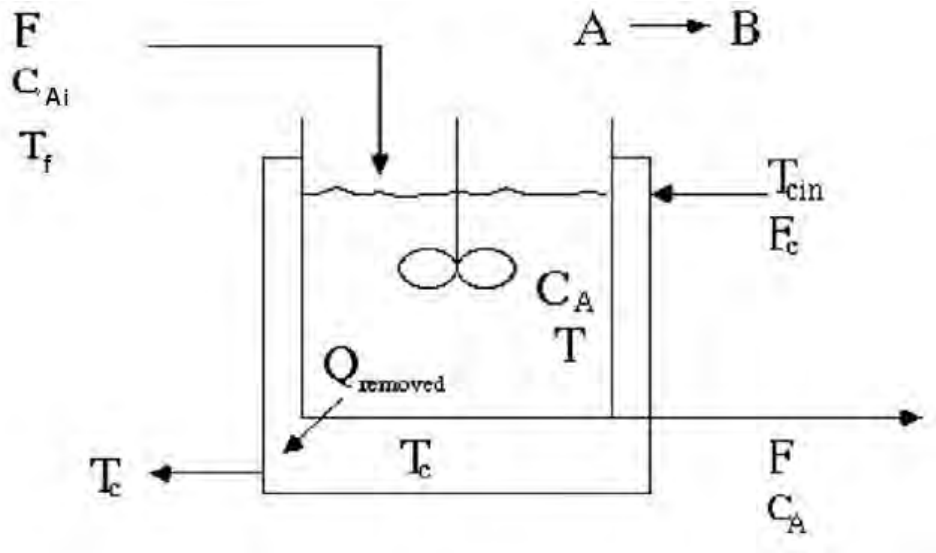

Figure 5.1: Schematics of a CSTR

The dynamic behavior of the system is represented by a set of differential equations, portraying the rate of change of concentration of reactants and temperature of the reactor respectively. The model equations are given by [30]:

$$\frac{dc_A}{dt} = \frac{F}{V}(c_{Ai} - c_A) - k_0 c_A e^{\frac{-E}{RT}} \tag{5.1}$$

$$\frac{dT}{dt} = \frac{F}{V}(T_f - T) - \frac{(-\Delta H)k_0 c_A}{\rho C_p} e^{\frac{-E}{RT}} + \frac{\rho_c C_{pc}}{\rho C_p V} q_c \left[1 - e(\frac{-hA}{q_c \rho_c C_{pc}})\right](T_c - T) \tag{5.2}$$

The values of the respective parameters along with their notations are taken from [25] and listed in Table 5.1. Steady-state values of 0.2645 $kmol/m^3$ and $393.9K$ for c_{A0} and T_{fi} are used respectively. The SIMULINK model of the process is shown in Figure 5.2. The inlet concentration, C_{Ai}, was excited by adding sinusoidal signals of varying frequencies and amplitudes to the steady-state feed concentration, C_{A0}. The outlet concentration data, c_A, were collected and subsequently used for nonlinearity quantification of the process.

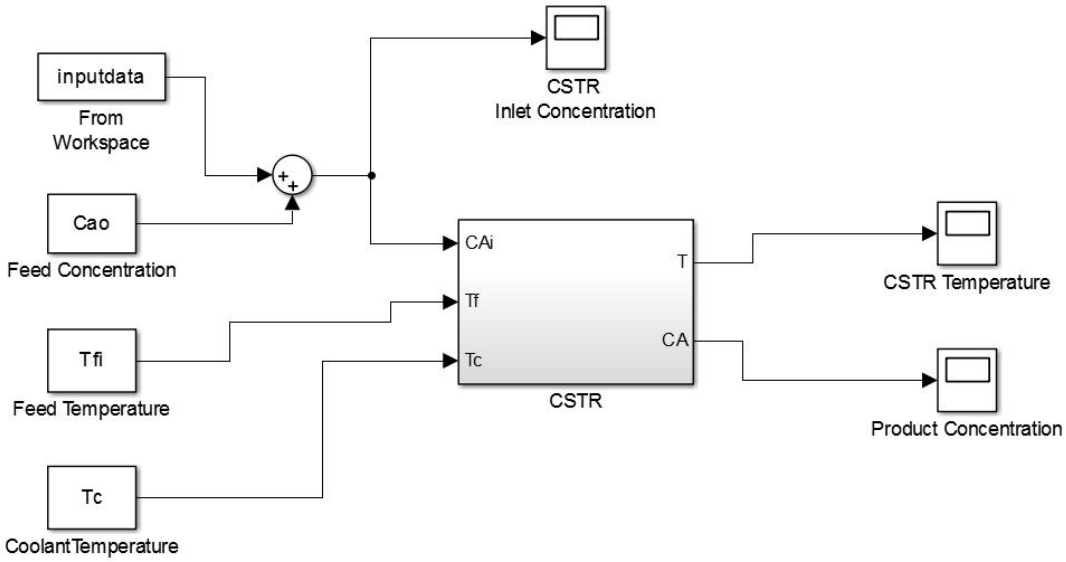

(a) External view of the SIMULINK Model of the CSTR Process

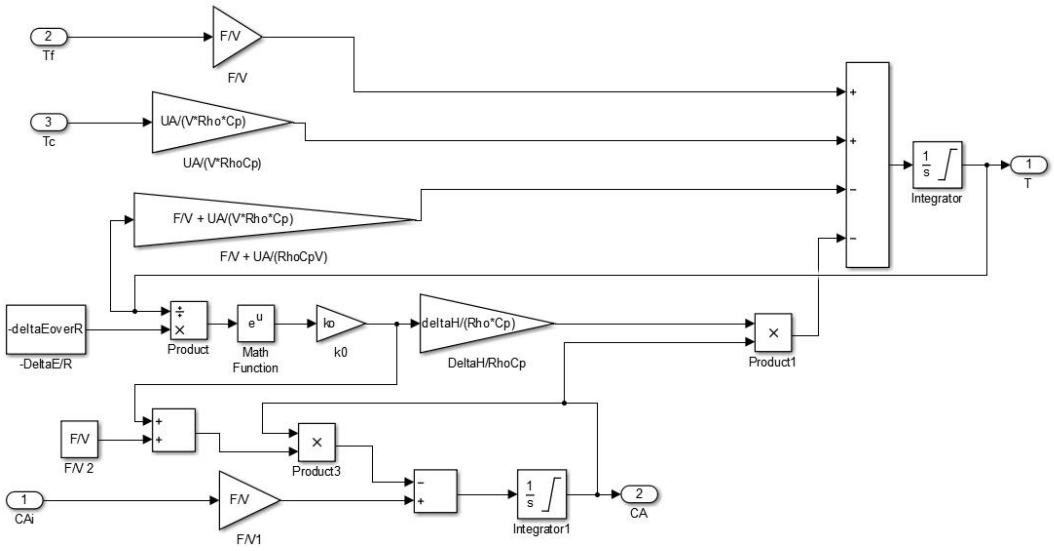

(b) Interior of the SIMULINK model of the CSTR block

Figure 5.2: SIMULINK model of the CSTR

5.1.2 Simulated Time Series Data of C_A

The input reactant concentration was varied using a sinusoidal signal. Figure 5.3 shows 20 of the output concentration time series data from the same CSTR for varying input concentrations. Multiple peaks in the power spectra of the output concentration data shows the presence of additional frequencies in addition to the one, used to excite the process, indicating the presence of nonlinearity in the CSTR. Therefore, the CSTR does not exhibit sinusoidal fidelity and the nonlinearity of the process is confirmed.

Parameter	Notation	Value
Inlet Feed Temperature	T_{fi}, T_i	323K
Inlet Coolant Temperature	T_c	365
Concentration of reactant	C_{A0}	2 $kmol/m^3$
Feed Flow-rate	F	1 m^3/min
Volume of the reactor	V	1 m^3
coolant flow-rate	F_c	15 m^3/min
density of coolant	ρ_c	$10^6 g/m^3$
Specific heat of cooling water	C_{pc}	1 cal/(g K)
density of the reactant and product	ρ	$10^6 g/m^3$
overall heat transfer co-efficient*Area	UA	$a * F_c^{(b+1)}/(F_c + \frac{a*Fc^b}{2*Rhoc*C_{pc}})$ a=$1.678 * 10^6$, b=0.5
Specific Heat of the product	C_p	1 $cal/(g^0C)$
activation energy/gas constant	$\frac{E}{R}$	8330.1 K^{-1}
reaction rate constant	k_o	$1.0 * 10^{10} min^{-1}$
Heat of reaction	ΔH	$-130 * 10^6 cal/kmol$

Table 5.1: Initializing parameters for CSTR model

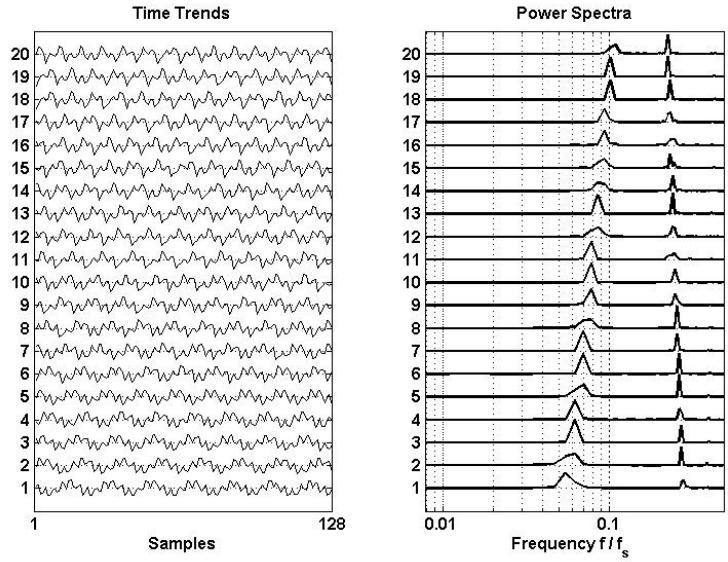

Figure 5.3: Output Concentration Data when Amplitude is set at 0.1 and frequency is increased (in order from bottom to top)

5.1.3 Nonlinearity Analysis Results

5.1.3.1 Bicoherence Based Results

Figure 5.4a shows that for small changes in amplitude, i.e., small changes in reactant concentration, the values of TNLI are close to zero (the lower left portion of the plot). This is expected, because for small excitations, the nonlinear processes can be assumed to be 'locally linear'. Thus TNLI is close to zero. As the amplitude increases, the nonlinearity goes up and so does the TNLI. The nonlinearity has increased monotonically with changes in frequencies and amplitudes. Thus, Total Nonlinearity Index increases with increasing frequency and amplitude.

When the range of oscillation for both amplitudes and frequencies are increased,

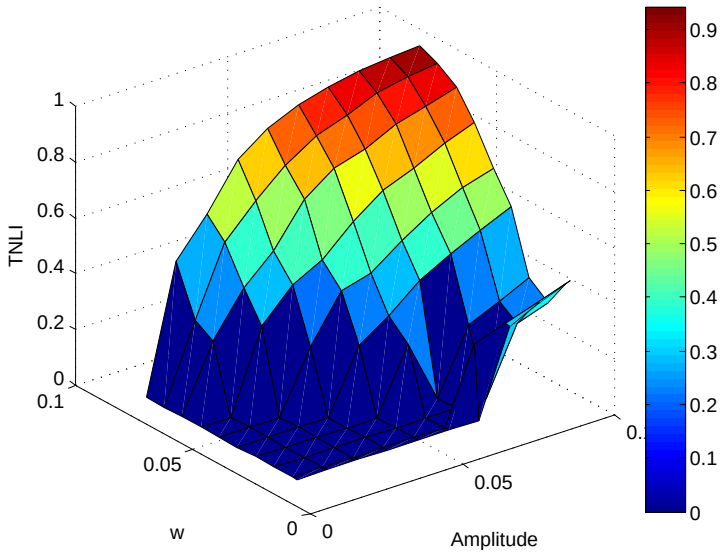

(a) Total Nonlinearity Index (TNLI) Pattern for CSTR

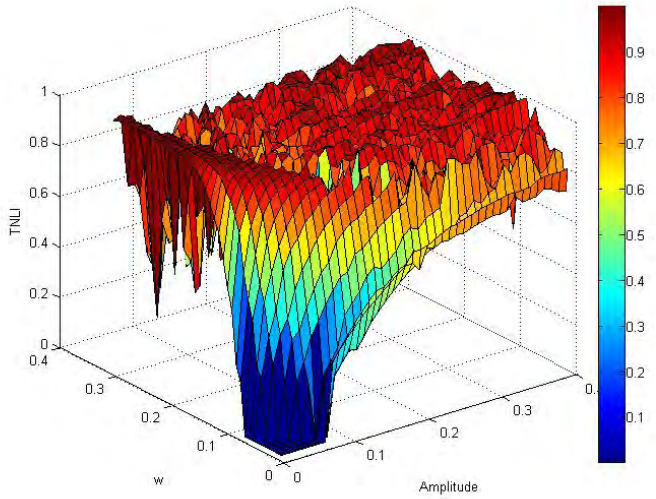

(b) Total Nonlinearity Index (TNLI) Pattern for CSTR with increased range of Frequency and Amplitude

Figure 5.4: Nonlinearity Analysis Results of CSTR with Bicoherence-based measure.

it is seen that TNLI stops increasing after exceeding a certain frequency irrespective of increasing amplitude. This is shown in the left portion of Figure 5.4b. Further increase of frequency shows a decrease in TNLI in the low amplitude region. This phenomenon may be attributed to the fact that above a certain threshold frequency, the CSTR acts as a *low-pass filter* and thus, the high frequency sinusoids are absorbed as high frequency disturbances as long as their amplitudes are small.

5.1.3.2 Surrogate Data based Results

Figure 5.5 shows the variation in N_{surr}, when Surrogate data-based measure is applied to the same data-set. As seen from the figure, N_{surr} does not monotonically increase with amplitudes and frequencies; rather, it generates an irregular pattern. The plot in Figure 5.5a shows that in the vicinity of lower amplitudes, the nonlinearity mostly increases with increasing frequency. N_{surr} does not increase much with the increase of amplitudes from 0.01 to 0.1, showing that N_{surr} is less sensitive for small incremental changes in amplitude. When the ranges of both amplitudes and frequencies are increased, it is seen that after the amplitude has crossed a threshold value, N_{surr} shows large peak in the high amplitude but low frequency areas. This is visible in the right portion of the Figure 5.5b.

In order to investigate the effect of noise on N_{surr}, gaussian white noise was added to the data and Surrogate Nonlinearity Index was recalculated. As shown in Figure 5.6, when some noise was added to the data, the pattern of N_{surr} changed. The change in N_{surr} for change in amplitude is now more prominent than for change in frequency,

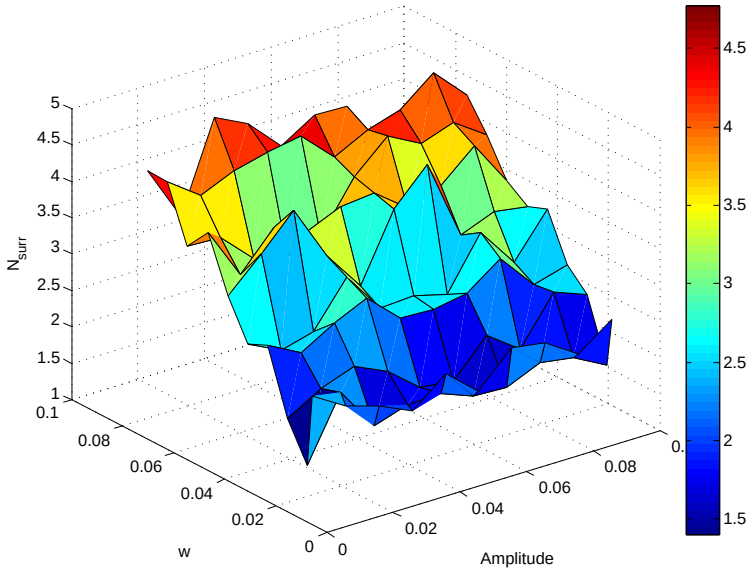

(a) Surrogate Nonlinearity Index (N_{surr}) Pattern for CSTR

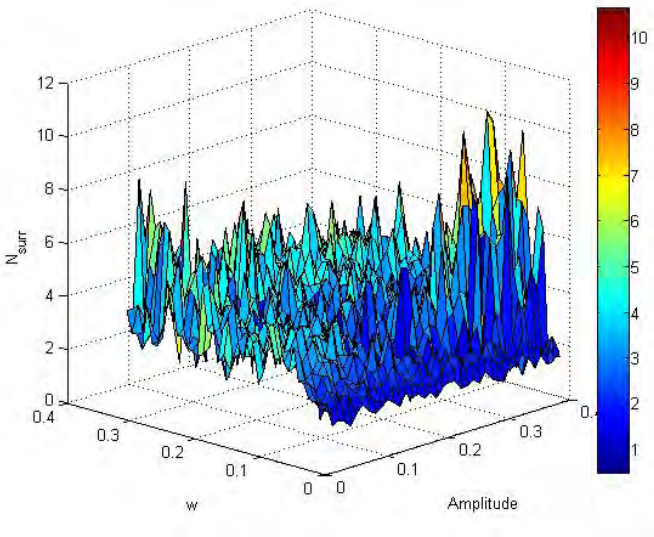

(b) Surrogate Nonlinearity Index (N_{surr}) Pattern for CSTR

Figure 5.5: Surrogate Data based Nonlinearity results for CSTR in absence of noise.

Figure 5.6a. When the range of variation of the variables is increased, as in Figure 5.6b, the pattern remains almost the same as before. However, in the latter case, the peaks

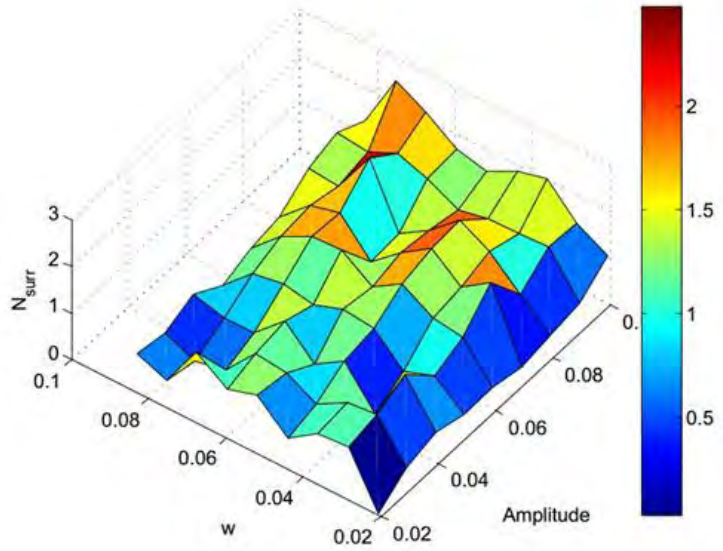

(a) Surrogate Nonlinearity Index (N_{surr}) pattern of a CSTR (with added noise)

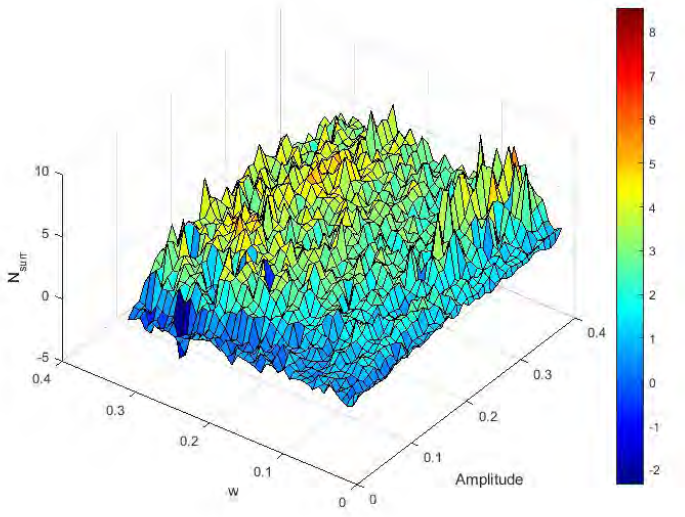

(b) Surrogate Nonlinearity Index (N_{surr}) pattern of a CSTR (with added noise) with increased range of Frequency and Amplitude

Figure 5.6: Surrogate Data based Nonlinearity results for CSTR in presence of noise.

are smaller than those for noise-free data.

While the plots of Total Nonlinearity Index appeared to be bounded between 0 and 1, plots of N_{surr} showed higher sensitivity to nonlinearity for small excitation signals and did not seem to be bounded.

5.1.3.3 Maximal Lyapunov Exponent Based Results

Results reported for TNLI and N_{surr} in the previous sections involve analysis of data for 1600 cases for an amplitude-frequency grid of 40×40. It is difficult to apply method of Maximal Lyapunov Exponent for such large data sets because the calculations involve visual identifications from plots. Evaluating a handful of points is not sufficient to generate a comprehensible pattern for Maximal Lyapunov Exponent . For the sake of comparison, the method is applied on two output time series, chosen randomly. The time series are chosen as such that they each registered high value for TNLI when quantified with Bicoherence-based measure.

Two output time series data are tested for nonlinearity using the method of Maximal Lyapunov Exponent. The 'Time Delay', 'Embedding Dimension' and 'Theiler Window' have been calculated as discussed in Section 4.1.2.3. For the sake of brevity, the details of the calculations are not shown here.

Figure 5.7 shows the plots of $exp(s)$ against Δn (Equation 3.16) for multiple embedding dimensions for the two time series. In Figure 5.7, both plots show regions of robust linear increase, hence showing that a positive value of Maximal Lyapunov Exponent exists for each of these curves.

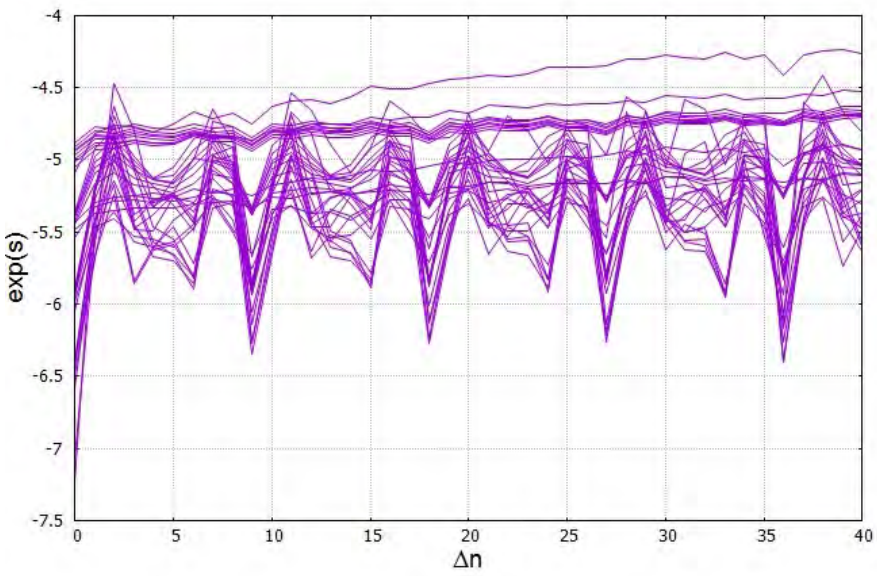

(a)

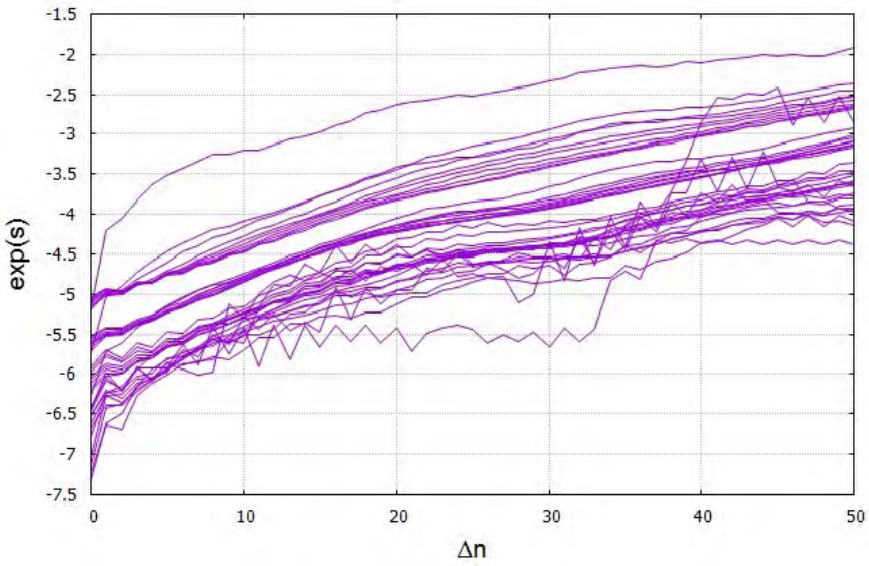

(b)

Figure 5.7: Analysis of Maximal Lyapunov Exponent for two output time series data from the nonlinear CSTR

Time Series	Time Delay	Embedding Dimension	Maximal Lyapunov Exponent
Figure 5.7a	9	3	0.00377
Figure 5.7b	2	10	0.0367

Table 5.2: Results of Maximal Lyapunov Exponent for two output time series from the nonlinear CSTR.

Table 5.2 summarizes the results of maximal Lyapunov method. It is seen that for highly nonlinear time series data from the CSTR, Maximal Lyapunov Exponent takes a positive value. The distinct linear regions in the curves, indicating a nonlinear system, may be attributed to the presence of exponential functions in the model of the CSTR. As seen from Table 4.6, Maximal Lyapunov Exponent is particularly sensitive to exponential function in addition to logarithmic and squared functions. More simulations are needed to carry out to discern the overall trend of Maximal Lyapunov Exponent with variation in amplitude and frequency.

5.1.3.4 Correlation Dimension Based Results

The same time series data of Section 5.1.3.3 are tested for nonlinearity using the method of Correlation Dimension.

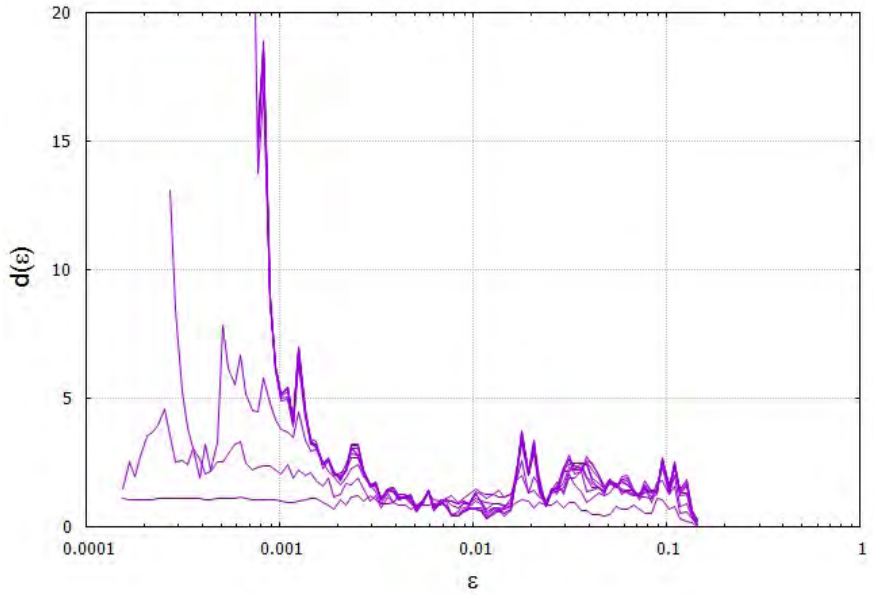

(a)

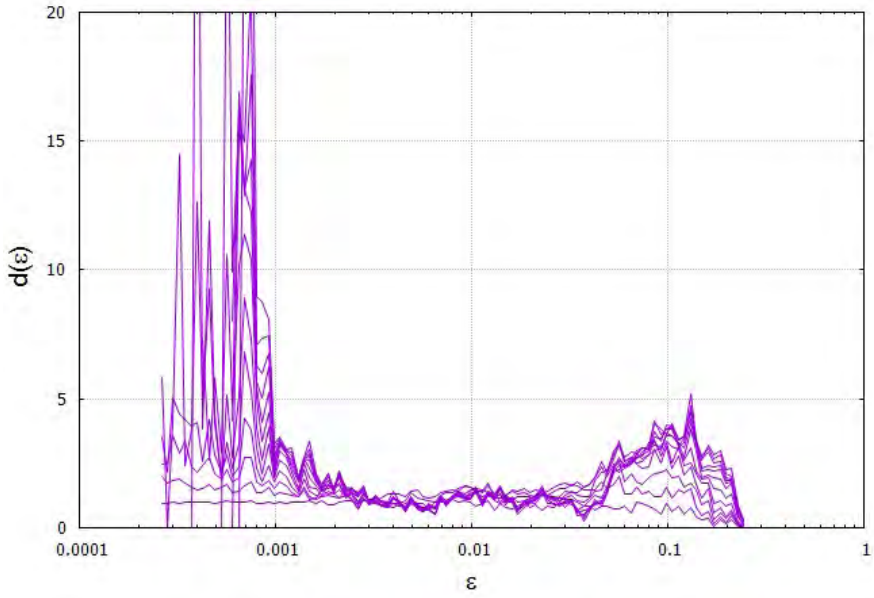

(b)

Figure 5.8: Analysis of Correlation Dimension for two output time series from the nonlinear CSTR

Figure 5.8 shows the plots of local slopes of the correlation integral, $d(\epsilon)$, against spatial separation, ϵ, (Equation 3.18), for multiple embedding dimensions for the two chosen time series. Both plots show onsets of plateau, hence showing that a positive value of Correlation Dimension exists for each of these curves.

	Time Delay	Embedding Dimension	Theiler Window	Correlation Dimension
Figure 5.8a	9	3	400	0.427
Figure 5.8b	2	10	400	1.20

Table 5.3: Results of Correlation Dimension for two output time series from the nonlinear CSTR.

Table 5.3 summarizes the results from the plots. It is seen that for highly nonlinear time series data from the CSTR, Correlation Dimension takes a positive value, indicating the presence of nonlinearity in the CSTR system. More simulations are needed to carry out to discern the overall trend of Correlation Dimension with variation in amplitude and frequency. It is to be noted that when exponential functions were driven by white noise in Chapter 4, Correlation Dimension yielded a value of 0. However, when the same function was included in the model equations of a chemical process and excited by sinusoidal variations, Correlation Dimension was able to detect nonlinearity in the system.

5.1.4 Summary of Nonlinearity Analysis

The following conclusions can be drawn from the simulation results:

(a) Bicoherence-based measure was able to show an increase in nonlinearity with increase in amplitude. It was also able to show that TNLI decreases after certain frequencies, indicating absorption of high frequency disturbances.

(b) Surrogate data-based measure appeared to be less sensitive for small changes in magnitude of excitation signals. In a noise-free data, Surrogate Nonlinearity Index showed a pronounced increase with respect to frequency rather than with respect to amplitude. It did show large peaks in the regimes with highest magnitude of amplitude when the range of amplitude is increased above a threshold value.

(c) Correlation Dimension could not be applied to all output time series because of its analysis involving visual observations. It had been used to quantify nonlinearity for two output time series data which also happened to register high values for TNLI. In both cases, Correlation Dimension gave positive results, indicating the presence of nonlinearity.

(d) Maximal Lyapunov Exponent also could not be applied to all output time series due to normal nature of analysis. It was used to quantify nonlinearity for the same two output time series data as Correlation Dimension. Maximal Lyapunov Exponent showed positive values, indicating the presence of nonlinearity in the concerned time series.

5.2 Nonlinearity Study of a Spherical Tank

5.2.1 Process Description

The second model is that of a spherical tank. Fig 5.9 represents a spherical tank of radius, R, where water enters from the top and leaves through a pipe at the bottom at a height of h_o from the base of the tank.

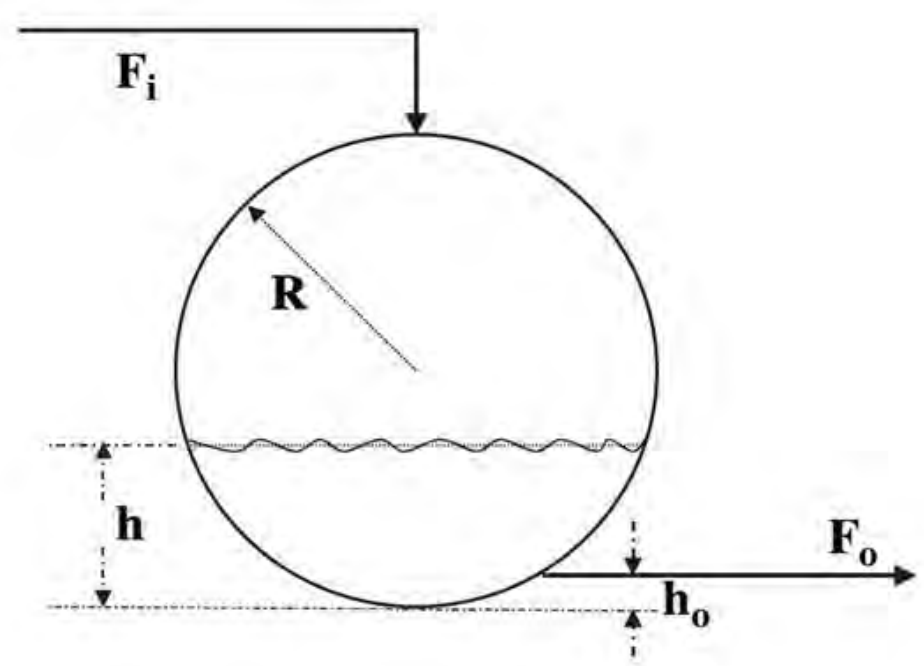

Figure 5.9: Schematics of a Spherical Tank

The model equation is as follows:

$$\pi R^2 \left[1 - \frac{(R-h)^2}{R^2}\right] \frac{dh}{dt} = F_i(t-d) - F_0(t) \tag{5.3}$$

Where $F_o(t)$ is the outlet flow rate at time t, h the height of the water level from the

bottom of the tank, and d corresponds to the delay in the input flow rate. The outlet flow rate, F_o, can be expressed as $F_o(t) = \sqrt{2g(h - h_o)}$, where g is the gravitational constant. For the open-loop simulation of the system, $R = 0.5$ m, $h_o = 0.01$ m have been used. The control of water level in the tank is accomplished by manipulating the inlet volumetric flow rate, F_i. Sinusoids of varying amplitudes and frequencies are added to the inlet volumetric flow and the water level is quantified for nonlinearity in each case.

The experiment is operated at a steady-state height of $0.35\ m$ of water in the tank so that the water in the tank neither dries out nor overflows. Also the water level behaves in a more nonlinear fashion at this height than while operating at the center of the tank.

The model of the spherical tank is created in SIMULINK.

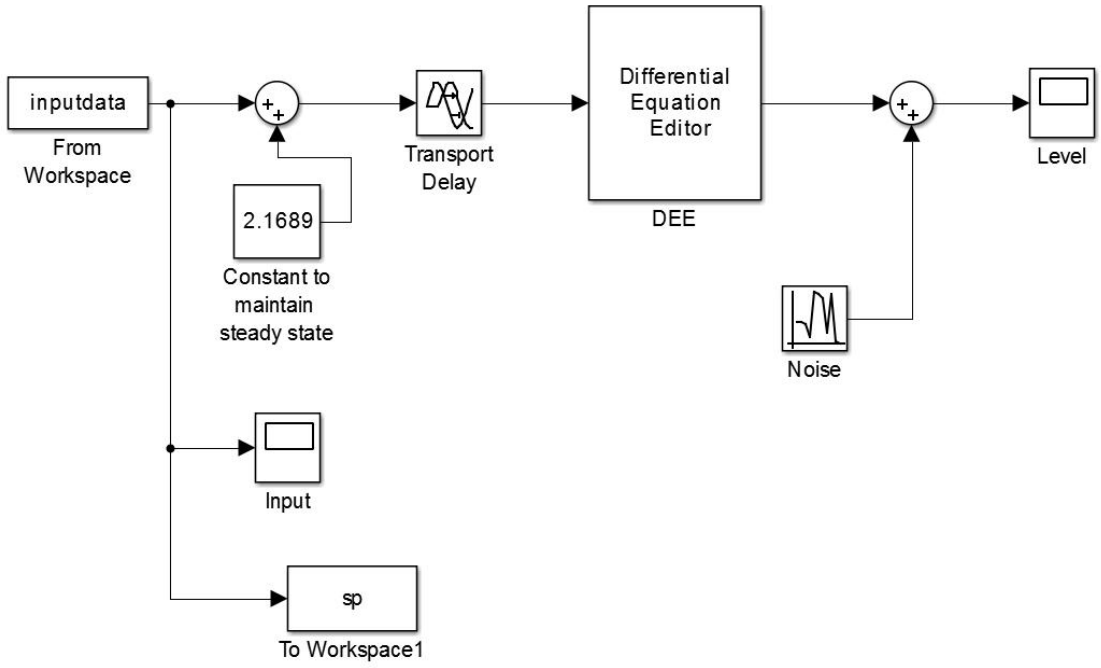

Figure 5.10: Simulink Model of the Spherical Tank

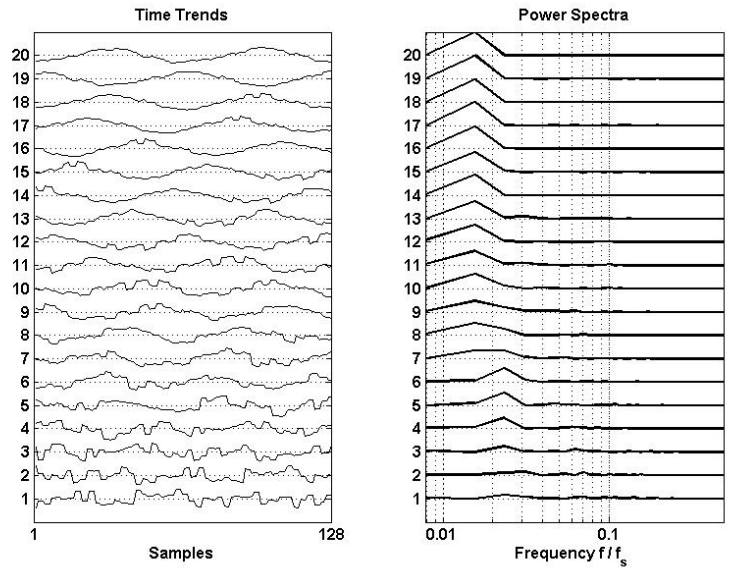

Figure 5.11: Data Samples when Frequency is set at 0.0738 rad/s and Amplitude is varied from 0.01 to 0.02

5.2.2 Simulated Data

The input signal is the same as that in Figure 3.1. Thus, the input signal has only a single frequency. The High Density Plot for a series of data with a fixed frequency but varying amplitude are given in Figure 5.11. The Figure shows that for small amplitudes of oscillation, the system can be considered as 'locally linear'. This is shown by the absence of peaks in the power spectrum when the amplitude is very small (Tags 1 and 2). The corresponding time trend is mostly noise. As the amplitude of oscillation is steadily increased, peak starts to appear in the power spectrum and the size of the peak increases with increasing amplitude of oscillation showing the sensitivity of the system to changes in amplitude.

5.2.3 Nonlinearity Analysis

5.2.3.1 Bicoherence Based Results

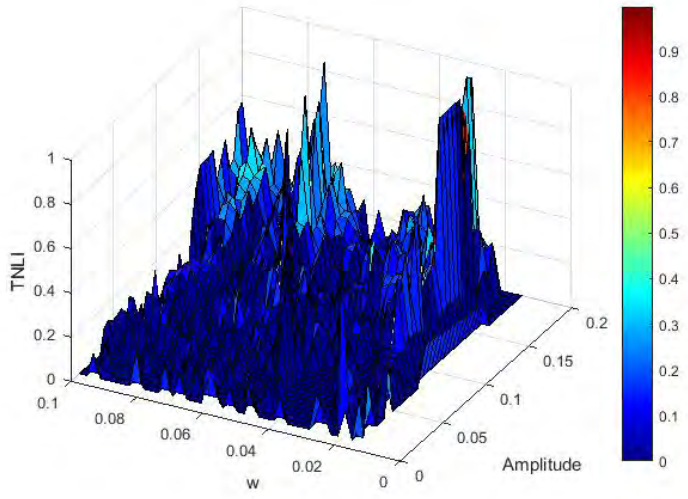

Figure 5.12: Total Nonlinearity Index (TNLI) Pattern for Spherical Tank

Figure 5.12 shows that for small magnitudes of input signals, the spherical tank system can also be assumed locally linear as portrayed by the flat regions on the lower left portion of the plot of TNLI. As the amplitude of excitation signal increases beyond a certain value, nonlinearity suddenly jumps as visualized from the several peaks at the right portion of the plot. The reason for this can be attributed to the fact that nonlinearity increases at a point where the total surge volume of the tank drops below a certain level. With the decrease in liquid volume, the tank loses its ability to attenuate disturbances, and thus it contributes to an increase in TNLI. Another fact is that the curvature of the spherical tank increases when moved away from the center along the top or bottom

direction of the tank. Thus the height of the same volume of water will behave in a more nonlinear fashion when operating closer to the top or bottom portion of the tank than it would while operating near the centre. It is also observed that the nonlinearity of this particular system is not very sensitive to changes in frequency. Therefore, it can be concluded that nonlinearity of the process depends on the size of the excitation signal.

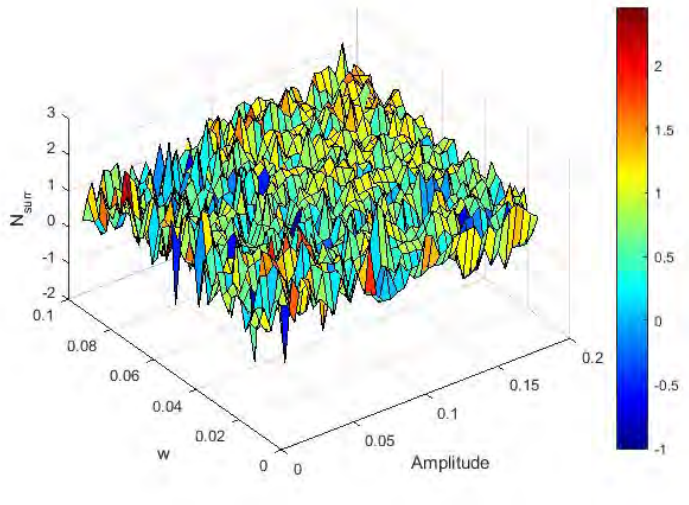

Figure 5.13: Surrogate Nonlinearity Index Pattern for Spherical Tank

5.2.3.2 Surrogate Data Based Results

The Surrogate data-based measure is applied to the same data-set. Figure 5.13 shows that nonlinearity is increasing with both frequency and amplitude. However, the rise in N_{surr} is roughly uniform. There is no presence of peaks similar to that in the plot of Total Nonlinearity Index. The absence of flat regions in the plot of Surrogate Nonlinearity Index shows its inability to find *'locally linear'* regions. The dependency of N_{surr} on

amplitude can be attributed to the fact as discussed previously.

5.2.3.3 Maximal Lyapunov Exponent Based Results

Two output data sets with high values for TNLI are chosen in random. No robust linear region has been found on the plots of $exp(s)$ against Δn (Equation 3.16) for multiple embedding dimensions for these time series. This shows that Maximal Lyapunov Exponent is not applicable for the spherical tank system. The reason can be attributed to the lack of exponential, logarithmic and squared functions in the model equation, to which Maximal Lyapunov Exponent is sensitive. By referring to Table 4.6, it is also evident that Maximal Lyapunov Exponent was not suitable for quantifying nonlinearity of purely sinusoidal functions.

5.2.3.4 Correlation Dimension Based Results

The same two output time series data were used to quantify nonlinearity using Correlation Dimension. The 'Time Delay', 'Embedding Dimension' and 'Theiler Window' have been calculated as discussed in Section 4.1.2.3.

Figure 5.14 shows the plots of local slopes of the correlation integral, $d(\epsilon)$, against spatial separation, ϵ (3.18) for multiple embedding dimensions for the two chosen time series. Both the plots show onsets of plateau (marked by circled regions), hence, showing that a positive value of Correlation Dimension exists for each of these curves.

Time Series	Time Delay	Embedding Dimension	Theiler Window	Correlation Dimension
Figure 5.14a	16	8	450	1.65
Figure 5.14b	12	6	400	1.63

Table 5.4: Correlation Dimension results for spherical tank system.

Table 5.4 summarizes the results from the plots. It is seen that for highly nonlinear time series data from the Spherical Tank, Correlation Dimension takes a positive value, indicating the presence of nonlinearity in the system. More simulations are needed to carry out to discern the overall trend of Correlation Dimension with variation in amplitude and frequency.

5.2.4 Summary of Nonlinearity Analysis

The following conclusions can be drawn from the results in this section.

(a) For a spherical tank system, Bicoherence-based measure is more sensitive to variation in amplitude of excitation signals. Unlike the uniform trend of increase in the case of CSTR, TNLI showed large peaks, portraying sudden increase in nonlinearity in case of the spherical tank system.

(b) Surrogate data-based measure shows an uneven increase in Surrogate Nonlinearity Index with respect to both frequency and amplitude. Unlike TNLI, which was more sensitive to amplitude, N_{surr} seemed to be more sensitive to both amplitude

and frequency.

(c) Maximal Lyapunov Exponent could not be calculated for the time series generated for this system. This may be attributed to the lack of logarithmic and exponential functions in the model equation of the spherical tank system.

(d) For time series with high values for TNLI, Correlation Dimension gave positive values. Further tests with different time series are required to identify the trend of Correlation Dimension with respect to amplitude and frequency.

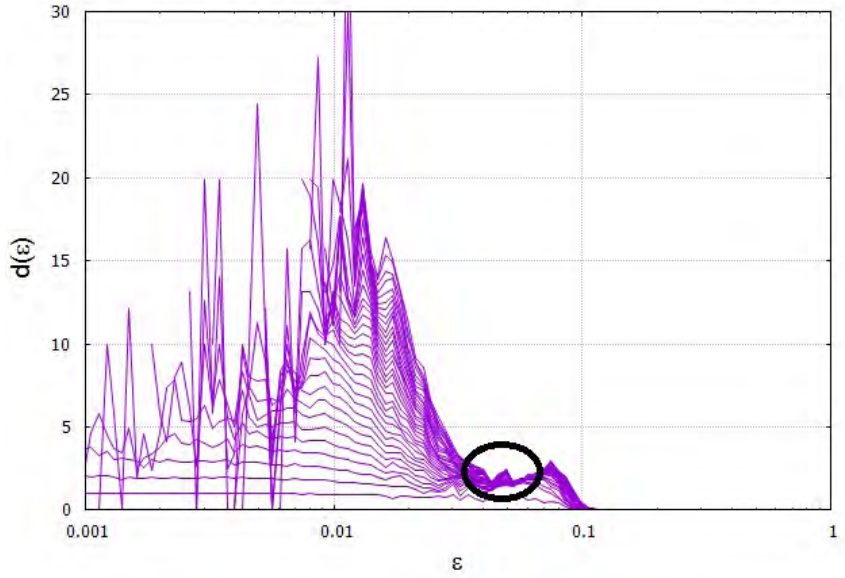

(a)

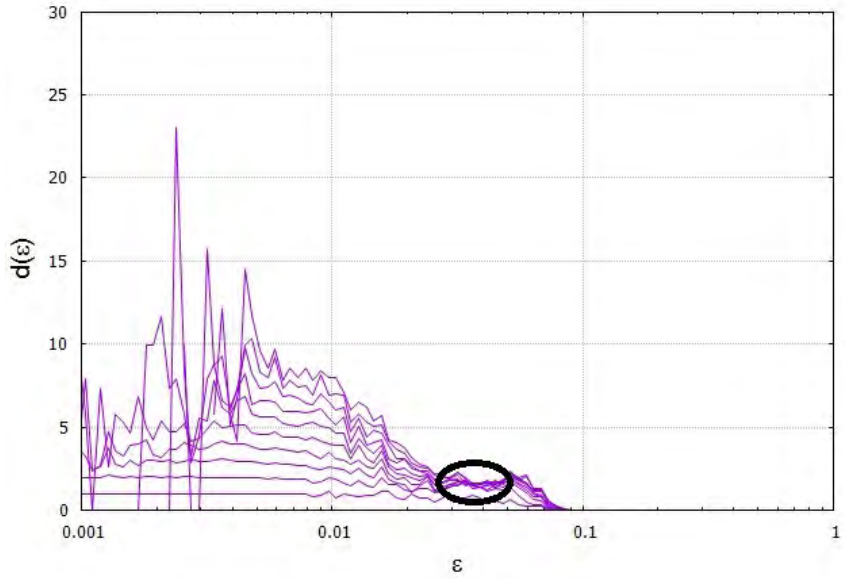

(b)

Figure 5.14: Correlation Dimension analysis of two output time series data from Spherical Tank.

CHAPTER 6

EFFECT OF CONTROLLER ON NONLINEARITY

To study the effect of controller on the nonlinearity of a system, the spherical tank system was simulated in closed loop condition. A PI controller was implemented to control the water-level of the spherical tank by manipulating input flow-rate. The PI controller settings, used in the simulation is:

$$C(z^{-1}) = \frac{0.3 - 0.1z^{-1}}{1 - z^{-1}} \tag{6.1}$$

For experimentation in closed-loop, a new steady-state height of $0.3\ m$ was chosen to incorporate more nonlinearity. The closed-loop model of the Spherical tank was created using MATLAB and SIMULINK and it is shown in Figure 6.1.

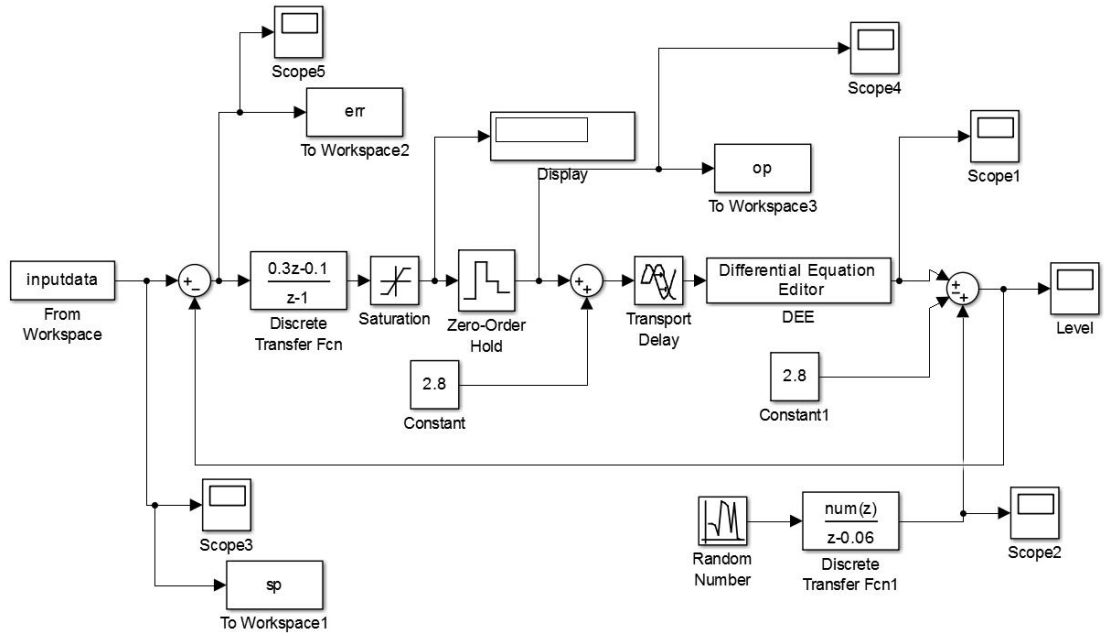

Figure 6.1: Closed-Loop Simulink model of the Spherical Tank

6.1 Simulated Data

The High Density Plot of the output dataset for the same input excitation signals is compared in both open loop and closed loop conditions in Figure 6.2. Unlike the case in open loop condition, in closed loop, there are peaks in Power Spectrum even when the amplitudes of oscillation are small. In addition to this, magnitudes of the peaks in the closed loop case appear to be smaller than those in open loop case. However, this fact is only moderately visible in the regions of high amplitudes and cannot be taken as a decrease in nonlinearity in closed loop condition.

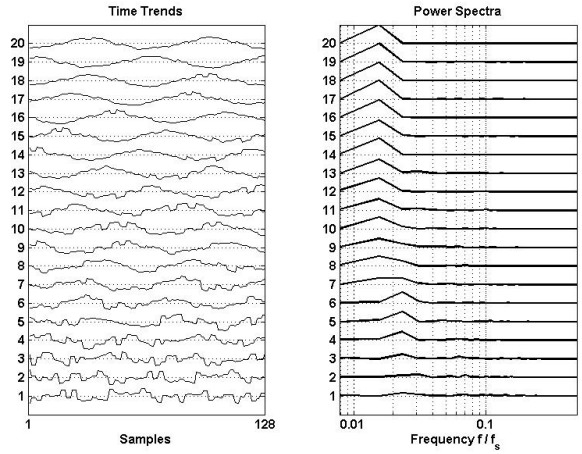

(a) Time Trend and Power Spectrum of Water Level Data in Open Loop

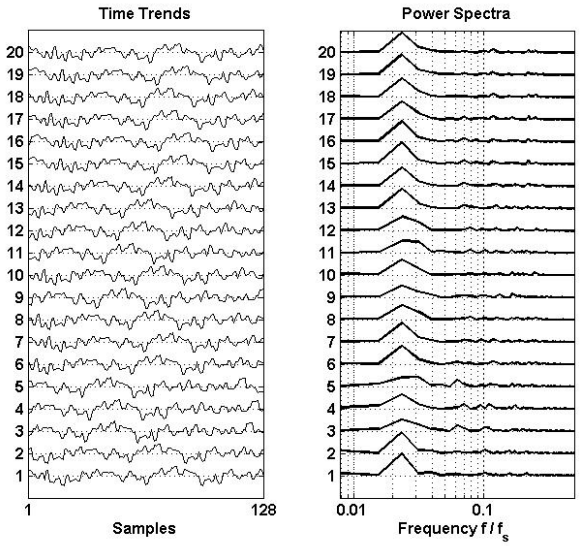

(b) Time Trend and Power Spectrum of Water Level Data in Closed Loop

Figure 6.2: High Density Plots comparing Output time series in both open loop and closed loop conditions.

6.1.1 Results with Bicoherence-based measure

Figure 6.3 shows the comparison of TNLI for the same output time series data from the spherical tank, operated in both open loop and closed loop Conditions.

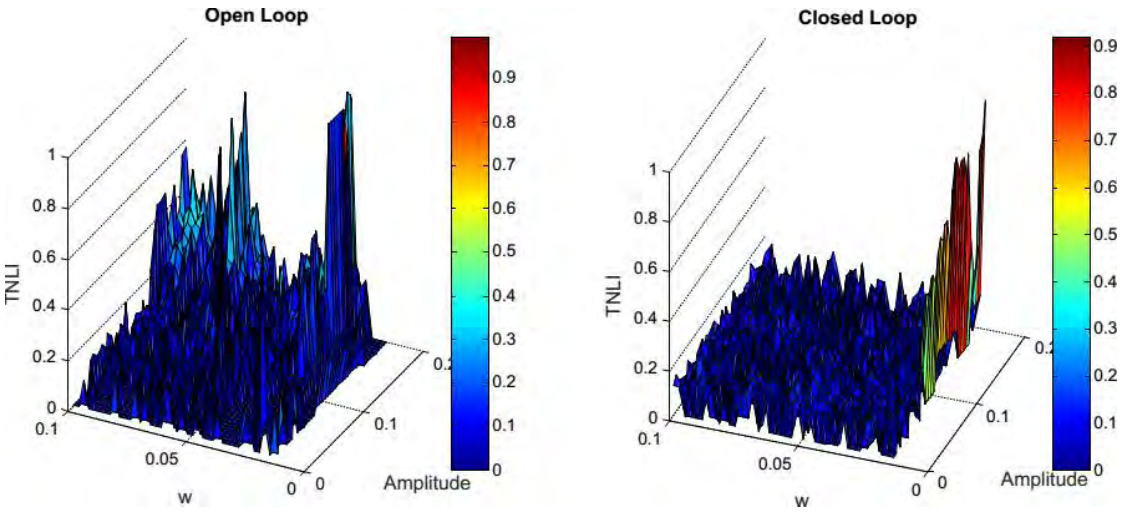

Figure 6.3: Comparison of Surface-plots of TNLI in Open Loop (Left) and Closed-Loop Conditions (Right)

TNLI plot for closed loop case shows less number of large peaks as compared to the open loop case, indicating some attenuation of nonlinearity. The absence of large peaks in the left portion of the plot indicates that for the same amplitude and frequency, the TNLI is smaller in closed-loop feedback configuration than in open loop case. Also, at high frequency, the nonlinearity does not increase with the increase of amplitude because the tank operates as a low-pass filter. Thus, it can be stated that PI controllers attenuate process nonlinearity to some extent.

6.1.2 Results with Surrogate Nonlinearity Index

The comparison of Surrogate Nonlinearity Index in both open loop and closed loop conditions are shown in Figure 6.4. The figure indicates that in case of closed loop, values of N_{surr} are lower than those in the former plot. This fact is more prominent in the upper left regions of the respective plots. In the upper left region of the open loop plot, maximum values of N_{surr} are equal to or greater than 1.5. In the same region of the closed loop plot, maximum values of N_{surr} are less than 1.5. However, the difference is not as clear as it is in case of Bicoherence-based measure.

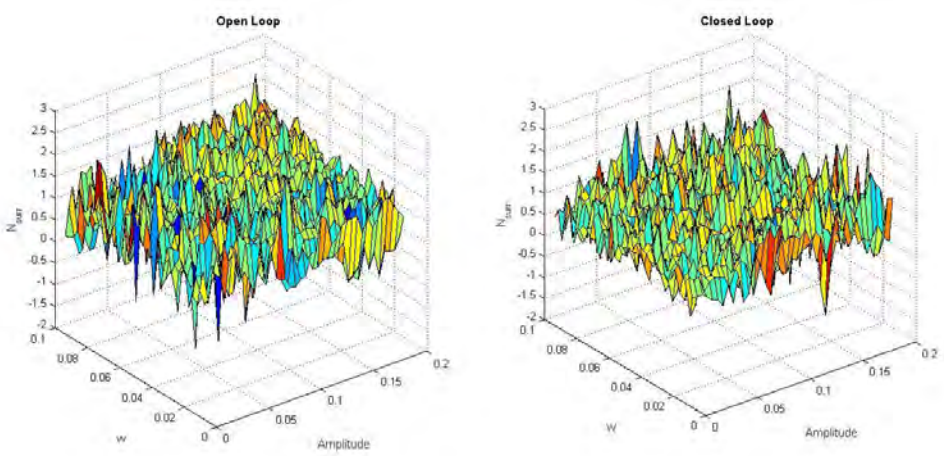

Figure 6.4: Comparison of Surface-plots for N_{surr} in Open Loop (Left) and Closed-Loop (Right) conditions

Since it is difficult to compare the above plots, the mean, variance and range of N_{surr} are calculated and compared in both open loop and closed loop conditions in Table 6.1:

,

	Mean	Range	Variance
Open Loop	0.848	3.46	0.245
Closed Loop	0.575	3.39	0.186

Table 6.1: Comparison of Mean, Range and Variance of N_{surr} for open loop and closed loop case of the spherical tank.

Table 6.1 shows that the values of mean, range and variance of N_{surr} are smaller in the case of closed loop than in open loop. So Surrogate data-based measure has also indicated a decrease in closed loop configuration.

6.1.3 Results with Correlation Dimension

The output time series data for the same input excitation is again studied in closed loop condition. The results are compared in Table 6.2:

	Time Delay	Embedding Dimension	Theiler Window	Correlation Dimension
Open Loop	16	8	450	1.65
Closed Loop	6	4	300	0

Table 6.2: Comparison of Correlation Dimension in open loop and closed loop

The same excitation signal that had registered a Correlation Dimension of 1.65 in open loop condition, registered a Correlation Dimension of 0 in closed loop condition. Thus method of Correlation Dimension also indicates a drop in nonlinearity in closed

loop configuration for the time series, generated from the given excitation signal. However, such might not hold true for other time series generated from different excitation signals in closed loop condition. A zero value indicates linearity which is not true. More output time series data, generated from different excitation signals, need to be quantified with the method of Correlation Dimension to be more conclusive.

6.2 Summary

From the simulations carried out in this chapter, it can be concluded that nonlinearity measures based on bicoherence, surrogate data, and Correlation Dimension have indicated that closed loop feedback controllers can attenuate process nonlinearity to some extent.

CHAPTER 7

EXPERIMENTAL EVALUATION OF NONLINEARITY MEASURES

In the previous chapters, nonlinearity measures were evaluated using simulated process data. This chapter evaluates nonlinearity measures using experimental data from a nonlinear conical tank system.

7.1 Nonlinear Water Level System

An experimental setup of a water tank level system is available in the Department of Chemical Engineering, BUET. The experimental data from this setup has been used to examine the efficacy or sensitivity of nonlinearity measures for such systems. A photograph of the water tank system is shown in Figure 7.1. As shown in the right panel of the same figure, a conical section has been inserted inside the tank to introduce nonlinear effect in the water level. The nonlinearity effect is due to the changes in gain of the

system as water level varies.

Figure 7.1: Physical Appearance of the Conical Tank

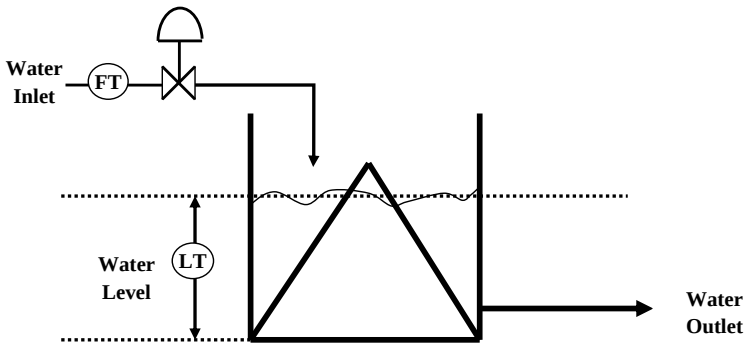

Figure 7.2: Schematics of the Conical Tank.

The water level in the tank is varied by manipulating the inlet volumetric flow rate. The schematics of the setup is shown in The water level is measured through a differential pressure transducer.

In this experiment, the input flow-rate is sinusoidally excited through application of

signals of various frequencies to the control valve and the water level data is recorded and used for nonlinearity quantification.

7.2 Time Series Data

The inlet flow-rate of water was excited with sinusoidal signal of periods of 400s, 300s, 200s, 100s and 50s respectively. The left panel of Figure 7.3 shows the water level data for five experimental runs. The lower data corresponds to sinusoidal excitation of a period of 400 s while the topmost for 50 s. The signal with a sinusoidal excitation of period of 50 s is of high frequency signal and it contains mainly noise. The right panel of Figure 7.3 shows the power spectra of the experimental data. The power spectra show the power or energy of the signal at various frequency of the signal. For example, the lowermost plot shows a peak at a frequency of 0.0025 Hz corresponding to a period of 400 s. Since the process was excited using a sinusoid with a period of 400 s, the power spectrum clearly shows the energy content of the water level data for this experiment is mainly at this period of 400 s or at a frequency of 1/400 or 0.0025 Hz. Similarly, the other power spectra show peaks at the frequencies of maximum energy content.

7.3 Nonlinearity Analysis Results

7.3.1 Bicoherence Based Results

Bicoherence-based measure was quantified for all data sets and the results are shown in Table 7.1. Ideally it would be expected that a particular system should have a constant

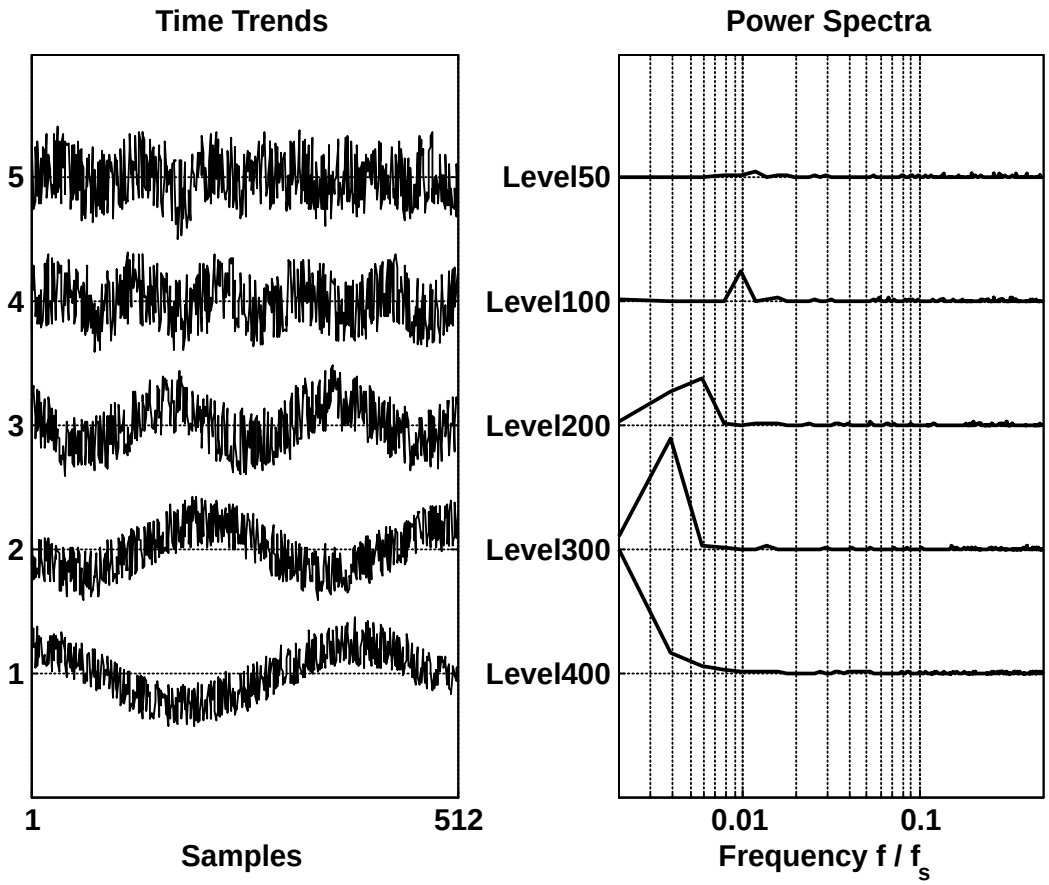

Figure 7.3: Time trends and Power Spectra of Water Level Data for conical tank system.

nonlinearity. However, in reality, it is not true. As shown in Table 7.1, Bicoherence-based measure depicts an increase in nonlinearity with decreasing frequency (or increasing period) of oscillation. The decrease in TNLI with increasing frequency can be attributed to the fact that the large volume of water in the tank absorbs the high frequency signals or noise and passes the low frequency signals.

From this, two conclusions can be drawn:

1. The nonlinearity of the system depends on the amplitude of the excitation signals.

Period (s)	Frequency (Hz)	TNLI
400	0.0025	18.1
300	0.0033	14.36
200	0.005	4.34
100	0.01	3.73
50	0.02	0.95

Table 7.1: TNLI results for experimental data from Nonlinear Conical Tank system

2. The tank process can act as a low pass filter and can absorb high frequency noise or disturbance.

7.3.2 Surrogate Data Based Results

Surrogate Nonlinearity Index was calculated using the same data. The results are tabulated in Table 7.2.

From Table 7.2, it is observed that Surrogate Nonlinearity Index shows consistent results for level data corresponding to periods of 200 s, 100 s and 50 s. The index was decreasing from 0.85 to 0.28 for increasing frequency as expected. However, for long oscillatory signals such as data corresponding to periods of 300 s and 400 s, the surrogate based nonlinearity index shows erroneous results. From this observation, it may be said that surrogate data method is not very suitable for nonlineairty quantification for very long oscillatory signals.

Period (s)	Frequency (Hz)	N_{surr}
400	0.0025	0.39
300	0.0033	-0.37
200	0.005	0.85
100	0.01	0.63
50	0.02	0.28

Table 7.2: N_{surr} results for the Nonlinear tank system.

7.3.3 Maximal Lyapunov Exponent Based Results

The graph of exponential form of ΔS against Δn (Equation 3.16) is plotted for multiple embedding dimensions in Figure 7.4. None of the plot shows the presence of a region with a constant positive gradient. Thus Maximal Lyapunov Exponent does not exist for these data-sets. To be considered as 'robust linear increase', a slope of constant gradient should exist for multiple data points. However, all the plots in Figure 7.4 showed a linear increase up to the first data point only. This cannot be regarded as a robust linear increase [22]. Thus, Maximal Lyapunov Exponent is not suitable for quantifying nonlinearity for these data sets. This result further corroborates the fact that Maximal Lyapunov Exponent is not suitable for processes with no logarithmic, exponential or squared terms, (also shown in Section 5.2). Therefore, Maximal Lyapunov Exponent method is unable to quantify nonlinearity of the water level data.

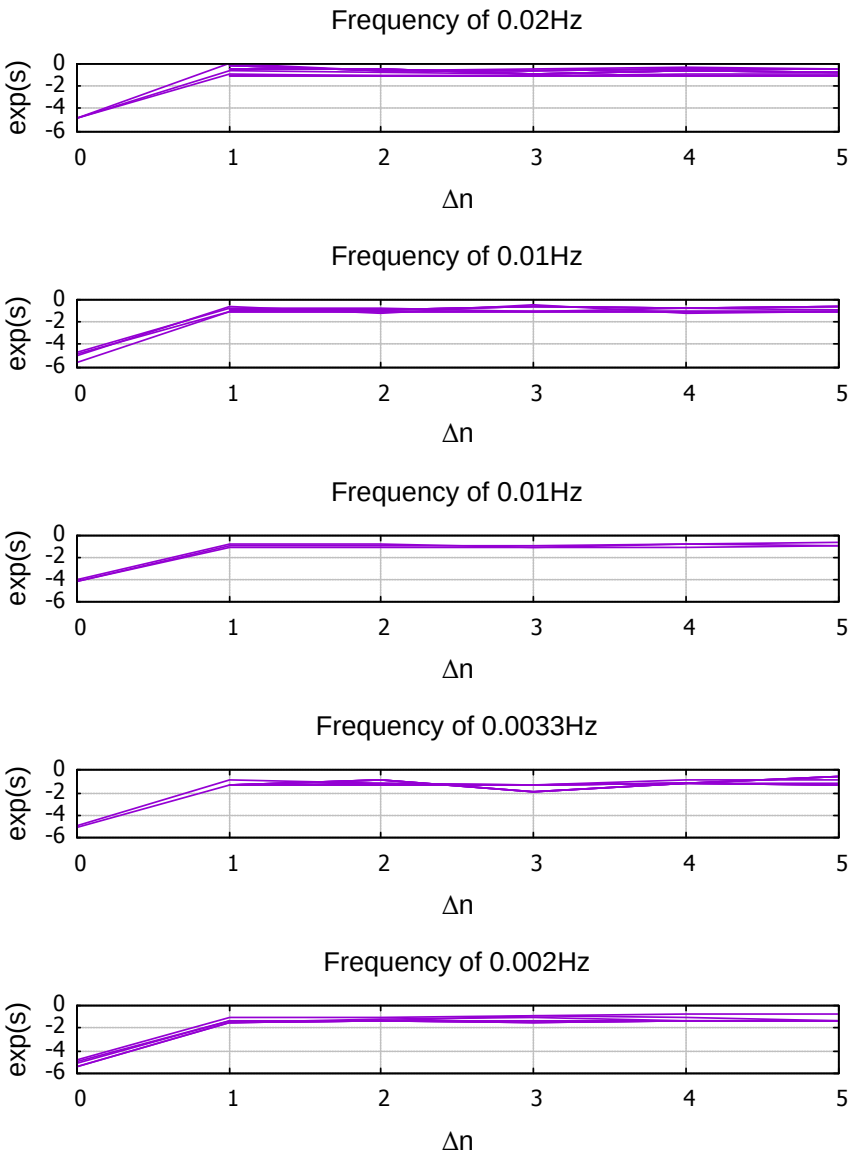

Figure 7.4: Plots for computing Maximal Lyapunov Exponent for nonlinear tank system

7.3.4 Plots for Calculation of Correlation Dimension

For the five data sets, plots of local slopes of Correlation Integrals, $d(\epsilon)$, (Equation 3.18), are plotted against spatial distance, (ϵ), and each curve corresponds to one of the multi-

ple values of embedding dimensions for which the curves are plotted. The procedure to get the Correlation Dimension from such plots is shown with an example in Figure 3.3 in Section 3.5.

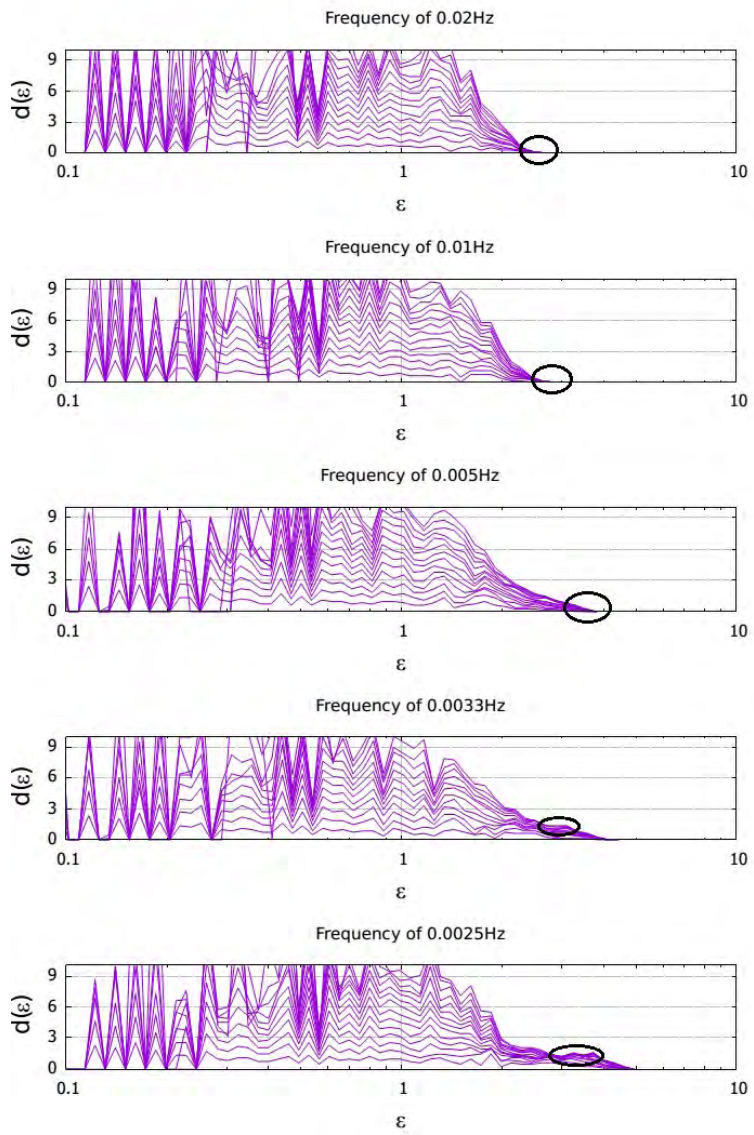

Figure 7.5: Plots of Local slopes of Correlation integrals against spatial separation distance for nonlinear tank system. (Period of signal increases from top to bottom)

Period (s)	Frequency (Hz)	Correlation Dimension
400	0.0025	1.8
300	0.0033	1.5
200	0.005	0
100	0.01	0
50	0.02	0

Table 7.3: Results of Correlation Dimension for experimental water level data

Taking Figure 3.3 as a reference, it is observed that in Figure 7.5, the plots corresponding to frequencies of 0.0025 Hz and 0.00333 Hz (periods of 400 s and 300 s respectively) are the ones that show flat regions in the positive y-axis (on the right side of the curves). The numerical values of Correlation Dimension estimated for these two data sets are 1.80 and 1.50, respectively. The flat regions for the other three plots are observed to be coinciding with the x-axis and thus are taken to be zero. Thus it can be said that in the case of the given data set on water level, Correlation Dimension decreases with increasing frequency or decreasing period. The results have been summarized in Table 7.3.

7.3.5 Overall Comparison

Nonlinearity measures based on Bicoherence, Surrogate Data, Correlation Dimension and Maximal Lyapunov Exponent are compared in Table 7.4.

Window	Period (s)	Frequency (Hz)	TNLI	N_{surr}	Correlation Dimension	Maximal Lyapunov Exponent
1	400	0.0025	18.10	0.39	≈ 1.8	not suitable
2	300	0.0033	14.36	-0.37	≈ 1.5	not suitable
3	200	0.005	4.34	0.85	0	not suitable
4	100	0.01	3.73	0.63	0	not suitable
5	50	0.02	0.95	0.28	0	not suitable

Table 7.4: Summary of results of four Nonlinearity Measures on experimental output data from Conical Tank

From Table 7.4, it can be concluded that the Bicoherence based method shows a constant increase in nonlinearity with increase in period which also translates as a decreasing trend in TNLI with increase in frequency of the excitation signal. The decrease in nonlinearity with higher frequencies can be attributed to the tank being behaving as a low-pass filter thus absorbing high frequency disturbances. Thus, Bicoherence-based measure is deemed to be the best choice for quantification of nonlinearity for the conical tank system.

For frequencies higher than 0.05 Hz or periods lower than 200 s, N_{surr} shows similar trend in results as compared to Bicoherence-based measure. However, suitability of N_{surr} for quantifying nonlinearity of data with long period of oscillation is debatable. More data sets for varying frequency is required to conclude on this aspect.

Maximal Lyapunov Exponent is not a suitable method for quantifying nonlinearity

for these data sets. This experiment further corroborates the fact that Maximal Lyapunov Exponent might not be a suitable measure of nonlinearity for chemical and/or physical processes in which no logarithmic, exponential or squared terms appear in the model equations.

Correlation Dimension shows an increasing trend with increasing period of oscillation; so it can be said that it also increases with increasing nonlinearity. But the degree of variation of Correlation Dimension appeared to be very small with respect to variation of frequency or period of oscillation.

CHAPTER 8

CONCLUSIONS AND RECOMMENDATIONS

This chapter lists the contributions of the thesis and recommendations for future work.

8.1 Conclusions

For most process plants, it is arduous to apply model based method for quantifying nonlinearity. Most plants have sophisticated process structure and consist of numerous control loops. Thus, it becomes difficult to use model based methods for identification or diagnosis purpose. Therefore, data driven methods are becoming increasingly popular because of its cost-effective nature. This thesis attempted to study and evaluate the performance of data-based methods for quantifying nonlinearity.

The major contributions of this thesis can be summarized as follows:

- Four data-based methods for quantification of nonlinearity, namely, Bicoherence-based measure, Surrogate Nonlinearity Index, Correlation Dimension, and Maximal Lyapunov Exponent have been discussed and illustrated with examples.

- The performance of various data-based nonlinearity measures have been evaluated for commonly used nonlinear mathematical functions, such as exponential, logarithmic, square and sinusoid, driven by white noise. It is found that the Bicoherence-based measure is suitable for quantifying nonlinearity of logarithmic and square functions. Maximal Lyapunov Exponent could quantify nonlinearity for all functions except sinusoids. Surrogate data-based measure is suitable for quantifying nonlinearity of sinusoidal and exponential functions. Correlation Dimension was not suitable for any of these functions when driven by white noise.

- The sensitivity of nonlinearity measures were examined using synthetic data generated by additive sinusoids and square type nonlinearity operator. It has been observed that Bicoherence-based measure was the most sensitive to the variation of degree of nonlinearity incorporated by the square operator. Surrogate data-based measure was partially successful in capturing the degree of nonlinearity. However, for highly nonlinear regions, it showed erroneous results. Maximal Lyapunov Exponent was not successful in quantifying nonlinearity of such sinusoidal signals. Correlation Dimension also failed to capture the true trend of the degree of nonlinearity.

- The data from the output of two simulated nonlinear processes namely, 'Contin-

uous Stirred Tank Reactor (CSTR)' and 'Spherical Tank' were used to find the suitability of the four data-based nonlinearity measures. Bicoherence-based measure was the most successful among them to capture the nonlinearity of the system. Surrogate data-based measure was next to the Bicoherence-based measure. Correlation Dimension and Maximal Lyapunov Exponent could qualitatively detect nonlinearity in the CSTR system. Maximal Lyapunov Exponent was not suitable for measuring nonlinearity in the Spherical Tank system because the model equation of the Spherical tank system does not contain any logarithmic or exponential terms.

- Effect of a controller on the nonlinearity of a process is studied. Three methods namely, Bicoherence-based measure, Surrogate data-based measure, and Correlation Dimension showed that feedback controllers can attenuate system nonlinearity to some extent.

- Finally, the performance of the four data based nonlinearity measures were evaluated by performing experiments in a pilot scale nonlinear conical tank system. Bicoherence-based measure could detect and quantify nonlinearity for all five experimental runs. The Surrogate data-based measure was successful for high frequency oscillations but failed for oscillations with long periods. On the other hand, Correlation Dimension was successful only for oscillations with long periods. Maximal Lyapunov Exponent was not suitable at all for these data sets.

It can be concluded that Bicoherence based Nonlinearity measure is the most suitable

method for nonlinearity quantification using process data.

8.2 Recommendations for Future Work

There are many things that could not be performed due to lack of time. The following are some of the issues that can be pursued further.

- Perform a comprehensive comparison of all nonlinearity measures.
- Perform simulation of various nonlinear processes such as pH process and other complex nonlinear processes and use the simulated data for evaluation of the performances of various nonlinearity measures.
- Develop a procedure for applying the nonlinear measures online in industrial processes to monitor system faults that may appear in the form of nonlinearity in data.
- The methods based on Correlation Dimension and Maximal Lyapunov Exponent currently requires visual determination of 'Time Delay', 'Embedding Dimension' and 'Theiler Window', which limits the application of these methods on large data sets. Both methods should be fully automated for making them suitable for large data sets.
- Extensive evaluation of nonlinear measures using experimental data from nonlinear pilot plants and industrial plants can be carried out.

REFERENCES

[1] Åström, K. J., Wittenmark, B., 2013. Computer-controlled systems: theory and design. Courier Corporation.

[2] Choudhury, M. A. A. S., Shah, S. L., Thornhill, N. F., 2004. Diagnosis of poor control-loop performance using higher-order statistics. *Automatica* 40 (10), 1719–1728.

[3] Choudhury, M. A. A. S., Shah, S. L., Thornhill, N. F., 2008. *Diagnosis of process nonlinearities and valve stiction: data driven approaches*. Springer-Verlag, Berlin Heidelberg, Germany.

[4] Choudhury, M. S., Shook, D. S., Shah, S. L., 2006. Linear or nonlinear? a bicoherence based metric of nonlinearity measure. In: *Fault Detection, Supervision and Safety of Technical Processes*. Vol. 6. pp. 617–622.

[5] Diks, C., Van Houwelingen, J., Takens, F., DeGoede, J., 1995. Reversibility as a criterion for discriminating time series. Physics Letters A 201 (2), 221–228.

[6] Eker, S. A., Nikolaou, M., 2002. Linear control of nonlinear systems: Interplay between nonlinearity and feedback. AIChE journal 48 (9), 1957–1980.

[7] Emara-Shabaik, H. E., Bomberger, J., Seborg, D. E., 1996. Cumulant/bispectrum model structure identification applied to a ph neutralization process. In: *UKACC International Conference on Control. Control '96*. IET, pp. 1046–1051.

[8] Fang, F., Tan, W., LIU, J.-z., 2005. Nonlinear output tracking control for the coordinated system of boiler-turbine units [j]. Proceedings of the Csee 1.

[9] Fang, F., Wei, L., 2011. Backstepping-based nonlinear adaptive control for coal-fired utility boiler–turbine units. Applied Energy 88 (3), 814–824.

[10] Fraser, A. M., Swinney, H. L., 1986. Independent coordinates for strange attractors from mutual information. Physical review A 33 (2), 1134.

[11] Friedmann, P. G., Stoltenberg, T. P., 1996. Continuous process control. Instrumentation Systems &.

[12] Guay, M., Dier, R., Hahn, J., McLellan, P., 2005. Effect of process nonlinearity on linear quadratic regulator performance. Journal of process control 15 (1), 113–124.

[13] Haber, R., 1985. Nonlinearity tests for dynamic processes. In: Proc. 7th IFAC Symp. Identification and System Parameter Estimation. pp. 409–414.

[14] Hegger, R., Kantz, H., Schreiber, T., 1999. Practical implementation of nonlinear

time series methods: The tisean package. Chaos: An Interdisciplinary Journal of Nonlinear Science 9 (2), 413–435.

[15] Helbig, A., Marquardt, W., Allgöwer, F., 2000. Nonlinearity measures: definition, computation and applications. Journal of Process Control 10 (2), 113–123.

[16] Hernjak, N., 2004. Control-relevant nonlinearity characterization. Ph.D. thesis, Ph. D. thesis, University of Delaware, Delaware, USA.

[17] Hernjak, N., Doyle, F. J., 2005. Glucose control design using nonlinearity assessment techniques. AIChE Journal 51 (2), 544–554.

[18] Hodgson, A., 1982. Problems of integrity in applications of adaptive controllers. Ph.D. thesis, University of Oxford.

[19] Hosseini, S., Fatehi, A., Johansen, T. A., Sedigh, A. K., 2012. Multiple model bank selection based on nonlinearity measure and h-gap metric. Journal of Process Control 22 (9), 1732–1742.

[20] Kantz, H., 1994. A robust method to estimate the maximal lyapunov exponent of a time series. Physics letters A 185 (1), 77–87.

[21] Kantz, H., Schreiber, T., 1997. *Nonlinear Time Series Analysis, vol. 7 of Cambridge Nonlinear Science Series*. Cambridge University Press, Cambridge, England.

[22] Kantz, H., Schreiber, T., 2004. *Nonlinear time series analysis*. Vol. 7. Cambridge university press, Cambridge, England.

[23] Lipták, B. G., Lipták, B. G., 1995. Process measurement and analysis. Butterworth Heinemann.

[24] Liu, J., Meng, Q., Fang, F., 2013. Minimum variance lower bound ratio based nonlinearity measure for closed loop systems. Journal of Process Control 23 (8), 1097–1107.

[25] Luyben, W. L., 1995. *Process modeling, simulation and control for chemical engineers*. McGraw-Hill Higher Education, New York, USA.

[26] Murrill, P. W., 1988. Application concepts of process control. Isa.

[27] Narendra, K. S., 2013. Adaptive and learning systems: theory and applications. Springer Science & Business Media.

[28] Nikias, C. L., Petropulu, A. P., 1993. *Higher-Order Spectra Analysis: A Nonlinear Signal Processing Framework*. PTR Prentice Hall, Englewood Cliffs, NJ.

[29] Paluš, M., Pecen, L., Pivka, D., 1995. Estimating predictability: redundancy and surrogate data method. arXiv preprint comp-gas/9507003.

[30] Pottman, M., Seborg, D. E., 1992. Identification of non-linear processes using reciprocal multiquadric functions. *Journal of Process Control* 2 (4), 189–203.

[31] Provenzale, A., Smith, L. A., Vio, R., Murante, G., 1992. Distinguishing between low-dimensional dynamics and randomness in measured time series. Physica D: nonlinear phenomena 58 (1), 31–49.

[32] Rosenstein, M. T., Collins, J. J., De Luca, C. J., 1993. A practical method for calculating largest lyapunov exponents from small data sets. Physica D: Nonlinear Phenomena 65 (1), 117–134.

[33] Schreiber, T., 1999. Interdisciplinary application of nonlinear time series methods. Physics reports 308 (1), 1–64.

[34] Schreiber, T., Schmitz, A., 1996. Improved surrogate data for nonlinearity tests. Physical Review Letters 77 (4), 635.

[35] Schreiber, T., Schmitz, A., 2000. Surrogate time series. *Physica D: Nonlinear Phenomena* 142 (3), 346–382.

[36] Schweickhardt, T., Allgöwer, F., 2007. Linear control of nonlinear systems based on nonlinearity measures. Journal of Process Control 17 (3), 273–284.

[37] Stack, A. J., Doyle, F. J., 1997. The optimal control structure: an approach to measuring control-law nonlinearity. Computers & chemical engineering 21 (9), 1009–1019.

[38] Theiler, J., Eubank, S., Longtin, A., Galdrikian, B., Farmer, J. D., 1992. Testing for nonlinearity in time series: the method of surrogate data. *Physica D: Nonlinear Phenomena* 58 (1), 77–94.

[39] Vlahogianni, E. I., Karlaftis, M. G., Golias, J. C., 2006. Statistical methods for detecting nonlinearity and non-stationarity in univariate short-term time-series of

traffic volume. Transportation Research Part C: Emerging Technologies 14 (5), 351–367.

[40] Zang, X., Howell, J., 2005. Correlation dimension and lyapunov exponent based isolation of plant-wide oscillations. In: *Dynamics and Control of Process Systems 2004 (IPV - IFAC Proceedings Volume)*. Elsevier, pp. 347–352.

[41] Zang, X., Howell, J., 2005. Isolating the root cause of propagated oscillations in process plants. *International Journal of Adaptive Control and Signal Processing* 19 (4), 247–265.